Title

HIGH-EHERGY NUCLEAR REACTIONS OF NIOBIUM WITH INCIDENT PROTONS AND HELIUM IONS

Author

Korteling, Ralph Garret.

Publication Date

1962-09-19

Thesis/dissertation

UCRL-10461

University of California

Ernest O. Lawrence
Radiation Laboratory

HIGH-ENERGY NUCLEAR REACTIONS OF NIOBIUM WITH INCIDENT PROTONS AND HELIUM IONS

Berkeley, California

DISCLAIMER

UCRL-10461

Research and Development

UNIVERSITY OF CALIFORNIA

Lawrence Radiation Laboratory
Berkeley, California

Contract No. W-7405-eng-48

HIGH-ENERGY NUCLEAR REACTIONS OF NIOBIUM WITH INCIDENT PROTONS AND HELIUM IONS

Ralph Garret Korteling
(Ph.D. Thesis)

September 10, 1962

Printed in USA. Price $2.25. Available from the
Office of Technical Services
U. S. Department of Commerce
Washington 25, D.C.

HIGH ENERGY NUCLEAR REACTIONS OF NIOBIUM WITH INCIDENT PROTONS AND HELIUM IONS

Contents

HIGH-ENERGY NUCLEAR REACTIONS OF NIOBIUM WITH INCIDENT PROTONS AND HELIUM IONS

Ralph Garret Korteling

(Ph.D. Thesis)

Lawrence Radiation Laboratory
University of California
Berkeley, California

September 10, 1962

ABSTRACT

High-energy nuclear reactions initiated by protons and helium ions on niobium have been investigated. Specific reaction products were selected to represent the low and high deposition-energy processes as well as the production of low-mass products. Excitation functions for these products were determined between the energies 240 to 720 MeV for incident protons, and 320 to 880 MeV for incident helium ions. The results from the proton bombardments were compared with values obtained from a Monte Carlo calculation of the cascade-evaporation model. The results from the proton bombardments were also compared with those from helium-ion bombardments.

In general, the comparison of experimental proton results with the results from the calculation gives satisfactory agreement for the low and high deposition-energy processes with the exception of specific cases such as the (p, pxn) reactions. This agreement might be improved with suitable refinements of the calculation. However, the calculation is not able to predict the production of low-mass products, and therefore another mechanism must be invoked to explain their production.

The comparison between the experimentally determined proton and helium-ion results shows a remarkable similarity. This similarity was unexpected from a consideration of high-energy processes such as meson production and interaction. The inconsistencies which arise from this observation are presented.

In addition, experimental information for the identification and decay properties of the previously unreported niobium-88 isotope is given.

I. INTRODUCTION

We investigate the behavior of protons and helium ions in high-energy nuclear reactions. The cascade-evaporation model of high-energy reactions that is discussed below predicts certain characteristic results for the interaction of protons with the nucleus. A comparison of these predictions with experimental observations is made. We find that the model is in agreement with a large part of the experimental information, but that certain features of the data, primarily the production of low-mass products, are not explained satisfactorily. A comparison of the experimental results from helium-ion and proton bombardments serves to indicate the behavior of the helium ions at high energies and the possible inadequacies of the models.

Niobium was chosen as the target material for three reasons: (1) it is mono-isotopic, which simplifies the interpretation of the results; (2) it yields a range of products which can be measured without the complication of fission; (3) it is a nucleus of sufficient complexity to permit a meaningful comparison to a statistical model and calculation. Selected reaction products were chosen as representative indicators of high-energy reactions; the selected nuclides were also chosen on the basis of experimental ease of measurement. We used niobium and zirconium nuclides to represent the products near the target that result from interactions of relatively low deposition energies. Copper and nickel nuclides were taken as representive products removed some distance from the target; large amounts of deposition energy are required to produce such nuclides. Low-mass products, for which we show that the cascade-evaporation model is inadequate, are represented by sodium nuclides. The formation cross sections for all these nuclides were determined with both projectiles as functions of bombarding energy.

Before we discuss these measurements and their results, we mention the general features of the cascade-evaporation model and its agreement with experimental results. This review indicates more clearly the

purposes of our study and the reasons for our approach to the problem. It is not intended that the following presentation be a complete analysis of the subject, but rather an informative discussion. Several excellent reviews[1-5] have summarized the available information, and the reader is referred to them for greater detail.

A. Cascade-Evaporation Model.

The Bohr[6] compound-nucleus model has found considerable success in explaining nuclear reactions induced by low-energy particles. It separates the process into two steps. First, the bombarding particle is absorbed into the nucleus with the formation of a compound nucleus at a well-defined excitation energy. Then, some time later, the compound nucleus de-excites by particle or gamma emission; this de-excitation is independent of the mode of formation for the compound nucleus. However, as the bombarding energy increases, the model ceases to explain the experimental data satisfactorily. The actual point of departure between the low-energy model and experimental data is not clearly defined and depends upon the mass of both the target and the bombarding particles. If protons are the projectiles, the Bohr compound-nucleus model begins to become inadequate at bombarding energies of 50 MeV, and by the time the energy is raised to 100 MeV, a major fraction of the reaction events do not involve compound-nucleus formation in the first step. Since we are investigating the high-energy region, we will restrict our discussion to mechanisms other than the Bohr compound-nucleus model.

The general features of the nuclear reactions observed in the first high-energy bombardments led Serber to postulate a two-step mechanism.[7] He observed that the interaction time between the projectile and nucleon within the nucleus is short compared to internuclear collision times. Therefore, the interaction of the projectile with the nucleus might be considered as occurring with the individual nucleons. However, since the momentum transfer in these collisions is not large in comparison

to the characteristic nucleon momentum ($\hbar/a$ versus $\hbar/d$, where "a" is the range of nuclear forces, and d is the mean separation of nucleons within the nucleus), these interactions could not be considered as simple collisions between free particles. The local interference which would be a feature of such a collison is a consequence of the degeneracy of nuclear matter and is an expression of the Pauli exclusion principle. However, if the nucleus is considered as a degenerate Fermi gas with the stipulation that following a collision both particles have a final energy greater than the maximum Fermi energy, the degeneracy of nuclear matter is taken into account and the interaction can then be considered as occurring between the projectile and the individual nucleon. This condition increases the mean free path of the projectile to the point where the probability of traversing the nucleus without interaction becomes finite; the nucleus is then said to become "transparent". When the projectile does collide with a nucleon, the average energy transfer is generally small. Thus, if the collision occurs near the nuclear surface, the projectile has a high probability of emerging with the majority of its energy. The struck nucleon, with its lower energy and consequently shorter mean free path, would have a high probability of undergoing further collisions until its energy is distributed among many nucleons. However, if the initial collision occurs near the center of the nucleus, the projectile has a greater probability of undergoing additional collisions and losing a greater percentage of its energy in a cascade of nucleons.

The first step of the Serber model can then be visualized as a fast ($\approx 10^{-22}$ sec) cascade of nucleons with a deposition of varying amounts of energy. This cascade process allows a complete spectrum of possible residual nuclei and excitation energies--from the case where a single collision has occurred with the deposition of a small amount of energy and the emergence of the projectile to the case where the majority of the incident particle energy is deposited and a number of nucleons are emitted.

The second step of the reaction, as postulated by Serber, was the de-excitation of the residual nuclei by the evaporation of particles in a process very similar to that of the de-excitation of the Bohr compound nucleus. As a consequence of the wide range of excitation energies and residual nuclei from the cascade process, the evaporation phase would then yield a large distribution of final products.

Miller and Hudis[1] have formalized the two-step mechanism for high-energy reactions by

$$\sigma(A,Z\,|A^0,Z^0,q,E) = \sum_{A,Z,I} \int_0^{\infty} \sigma(A',Z',U',I\,|A^0,Z^0,q,E)\,\eta(A,Z\,|A',Z',U',I)\,dU \qquad (I\text{-}1)$$

where $\sigma(A',Z',U',I\,|A^0,Z^0,q,E)$ is the differential cross section, in the cascade process, for the production of the residual nucleus (A',Z') which has spin I and excitation energy between U and U + dU, from the bombardment with projectile q having kinetic energy E on a target A^0,Z^0. The probability that the final product nucleus A,Z is produced in the evaporation process is then given by $\eta(A,Z\,|A',Z',U',I)$. This expression generalizes the model and extends the original hypothesis of Serber by placing no limitations on the cascade or evaporation steps. The sum over all possible nuclei produced in the cascade allows complete freedom in representing the initial step, and the η function allows the possibility of other modes of de-excitation than emission of small particles--namely, emission of larger units of nuclear matter and fission. However, the practical solution of the problem has required the use of the simplifying assumptions given by Serber.

The validity of the assumptions inherent in the Serber view of the cascade process has been examined by several people.[8-12] However, the semiqualitative presentation of Chew and Wick[11] is best suited for our purpose. They have treated the problem on the basis of three assumptions which we will refer to in total as the "impulse approximation". These assumptions are:

(1) The incident particle never interacts strongly with two constituents of the system at the same time.

(2) The amplitude of the incident wave falling on each constituent (nucleon) is nearly the same as if that constituent were alone.

(3) The binding forces between the constituents of the system are negligible during the decisive phase of the collision.

Consider an interaction to have a total cross section equal to its geometrical cross section and let this be set equal to $\pi\rho^2$ where ρ is the range of the fundamental interaction. If this geometrical cross section is taken to be approximately 30 mb, then $\rho \approx 1 \times 10^{-13}$ cm. Therefore, it can be seen that unless the mean radius separating the nucleons in the nucleus is $\geq 2 \times 10^{-13}$ cm, the first assumption becomes questionable. Thus, for an average nucleus where the mean radius is approximately 2.2×10^{-13} cm, the assumption is disputable.

The second assumption requires that the mean free path for the projectile be large in comparison to the dimensions of the interaction partner. If this is not the case, there will be an effective shielding by the other nucleons. Thus the condition $(3/4\pi)\sigma A^{1/3}/r_0^2 \ll 1$ is required where σ is the single nucleon cross section, and a constant nuclear density is assumed. If σ is again taken as approximately 30 mb, then $(3/4\pi)\sigma A^{1/3}/r_0^2 \approx (1/3)A^{1/3}$ and indicates that the second assumption is quite poor for complex nuclei.

Chew and Wick have estimated that if the average change in potential energy of the interaction is approximately 10 MeV and the bombarding energy is 200 MeV, the third assumption contains approximately 5% error.[11] This error becomes greater with decreasing bombardment energy but should not become unreasonable until the energy has dropped below 100 MeV.

Although the first two assumptions can lead to serious errors, the impulse approximation has of necessity been used in the solution of the cascade problem. Without its inclusion, the problem becomes

extremely difficult to solve. Its inclusion in the calculations has led to considerable success, although one is then tempted to question the results more critically.

B. Calculation of the Cascade Process.

The cascade process, as defined by Serber and denoted by $\sigma(A',Z',U',I|A^0,Z^0,q,E)$ in Eq. I-1, lends itself for solution to a statistical technique presented by Ulam and Von Neumann, more commonly known as the Monte Carlo method.[13] Goldberger initially formulated a quantitative representation of the cascade process by using the technique to determine the purely statistical aspects of the problem.[14] Subsequently, a number of these calculations have been performed with varying degrees of sophistication.[15-25] Our main interest in the following discussion will be to present only the general methods used in solving the problem. A more detailed discussion of one of these calculations[25] will be given in Sec. IV-A.

The Monte-Carlo technique for the solution of the problem is essentially a method of random selection of reaction parameters for a given case. Thus, the point of entry of the projectile into the nucleus, the distance it travels before collision, its collision partner, the momentum of the collision partner, the scattering angle, etc., are all determined through random choice. Once these parameters are chosen, the resultant kinematics of the collision are calculated. The process is repeated for a large number of events until sufficient statistical accuracy has been obtained to make the results meaningful.

For the results of the calculation to be physically meaningful, it is necessary to simulate conditions within the nucleus as accurately as possible. Generally, the nucleus is represented by a degenerate Fermi gas of nucleons in a nuclear square-well potential of radius $r_0A^{1/3}$. The Fermi gas is taken to be in its lowest-energy state and to remain there during the progress of the entire cascade. The Pauli

exclusion principle (or the degeneracy of nuclear matter) is accounted for by requiring that after collision both nucleons have energies greater than the maximum Fermi energy. Since the nucleons are considered to interact as modified free particles--modified in the sense that low-momentum-transfer collisions are excluded--the elementary cross sections needed for the calculation are taken to be the total p-p and n-p scattering cross sections. The mean free path of the particles can then be represented by

$$\lambda_i = \frac{(4/3)\pi R}{\rho \sigma_i} \alpha \qquad \text{(I-2)}$$

where $R = r_0 A^{1/3}$, ρ is the nucleon density in the nucleus, σ_i is the total scattering cross section for that specific case, and α is the fraction of collisions which are allowed. In like manner, the expressions for the probabilities of the other parameters of the collision (i.e., collision partner, momentum of collision partner, scattering angle, etc.) can be obtained. From a normalized plot of these probabilities, random numbers can select the parameters pertinent to an individual case and thereby represent the physical circumstances as well as possible.

A typical Monte Carlo calculation of the cascade process could proceed thus. A random number selects the point of entry of the projectile into the nucleus from a suitable plot of relative probabilities for specific areas. A second random number selects the distance which the projectile travels before collision from a plot of its mean free path. A third selects the collision partner, a fourth the momentum of the collision partner, and a fifth the scattering angle. With this information, the kinematics of the collision can be calculated. The results are tested to determine whether the collision is allowed. If it is not, the collision is discounted and a new collision point is selected. If it is, the information is tabulated and both particles are followed. In this way, a cascade can be followed until all collision partners have either been emitted from the nucleus or absorbed. The

excitation energy of the residual nucleus is then the sum of the "holes" in the Fermi gas and the excitation energy of the bound collision partners.

The information which such a calculation can provide is:

(1) The type, number, energy, and angular distribution of all emitted particles.

(2) The type, number, excitation energy, momentum, and angular distribution of all residual nuclei.

The validity of the results depends largely upon the degree of sophistication in the calculation. In the initial attempts of solving the problem, desk calculators were used and consequently a number of the components of the calculation were approximated. However, the success of the method in predicting the experimental data was such that Metropolis, Bivins, Strom, Miller, Friedlander, and Turkevich programmed the calculation for the MANIAC computer at the Los Alamos Scientific Laboratory.[24,25] It was then possible to eliminate the approximations made in the previous calculations and also to improve the statistical accuracy of the results. This calculation represents the best information available at the present time for the cascade process and is therefore taken as the basis of our view for this phase of the cascade-evaporation model. Since their results are used as a basis for a calculation of our own, we defer further discussion of their program until Sec. IV-A.

C. Calculation of the Evaporation Process

The second slower step of the Serber model is the de-excitation of the residual nuclei by particle emission, commonly referred to as the "evaporation process". The general basis for this process is the formalism for particle emission of the Bohr compound nucleus as derived by Weisskopf.[26,27] A number of workers have studied the problem from this point of view, notably Le Couteur,[28,29] Fujimoto and Yamaguchi,[30,31,32] and a series of authors who have been connected with the Monte Carlo Calculations.[33-38] An analytic solution can be obtained[28,30-32] if

several approximations are used, but a more satisfactory approach is to apply the Monte Carlo technique. We therefore concern ourselves with only the Monte Carlo method of solving the evaporation calculations. Since we will present an evaporation calculation later (See Sec. IV), only the general approach is given here.

Weisskopf's formalism for the probability $P(E)dE$ of a nucleus excited to the energy E emitting a particle with kinetic energy between E and E + dE is

$$P(E)dE = \frac{\sigma(E_i,E)gmEW_f(E_f)dE}{\pi^2\hbar^3 W_i(E_i)} , \qquad \text{(I-3)}$$

where $\sigma(E_iE)$ is the inverse cross section, $W_i(E_i)$ and $W_f(E_f)$ are the level densities of the initial and final nuclei, m is the mass of the emitted particle, and g is the number of spin states for that emitted particle. Since

$$E_i = E_f + E + Q_j, \qquad \text{(I-4)}$$

where Q_j is the separation energy of the emitted particle, the total probability is then

$$W(E_i) = \int_{}^{E_i-Q} P(E_j)dE_j = \frac{g\ m}{\pi^2\hbar^3} \int^{E_i-Q_j} \frac{\sigma(E_j)E_j - V_j)W_f(E_f)}{W_i(E_i)}\ dE_j, \qquad \text{(I-5)}$$

where V_j is the Coulomb barrier for the emitted particle suitably corrected for penetration.

The inverse cross section for neutrons is generally estimated by the geometrical cross section, πR^2, but for the cases of charged particle emission, the Coulomb barrier must be taken into account. Generally the cross section is set equal to zero for $E_j < V_j$, and equal to the geometrical cross section times the factor $(1 - V_j/E_j)$ for

$E_j > V_j$. An estimation of the level density requires a nuclear model. If the degenerate Fermi gas model is chosen for the evaporation process, the level density can be represented by

$$W(E) = \text{constant} \exp [2(aE)^{1/2}], \qquad \text{(I-6)}$$

where "a" is a parameter to be experimentally determined and taken to be of the form $a \propto A$. Hurwitz and Bethe have pointed out that the level density expression should be modified to take into account the odd-even pairing-energy effects and shell perturbations.[39] This feature can be incorporated into Eq. I-6 by addition of a constant factor, δ, which displaces the ground state. The level density is then

$$W(E) = C \exp 2 \ [a(E - \delta)]^{1/2} \qquad \text{(I-7)}$$

where C is a function of mass number but independent of energy. It must be noted at this point that the complete subject of level densities is poorly understood and that the foregoing description is only one representation.

The emission probabilities of any number of particles can then be calculated from Eq. I-5. Generally neutrons, protons, deuterons, tritons, helium-3, and helium-4 particles have been chosen, but the selection has been extended to include others[37,38]. The Monte Carlo technique consists of randomly choosing the evaporation chain for an excited nucleus. A random number selects the particle to be evaporated from a plot of their relative probabilities for emission. A second number selects the energy of the particle from a suitable distribution of energies. A product nucleus is thereby defined and the procedure repreated until a nucleus is reached which is unable to emit another particle. This nucleus is then taken to be the final product and a new evaporation chain is initiated.

The results of such a calculation are:

(1) The type, number, and energy distribution of emitted particles.

(2) The type, number, and residual energy of the final products.

Since the evaporation calculation uses the results of the cascade calculation as input information, any uncertainty in the initial cascade results will also be present in the evaporation results in addition to its own errors. Moreover, a question can be raised whether such an equilibrium mechanism is valid for an explanation of the de-excitation of the highly excited residual nuclei formed in the cascade process. This mechanism may have little physical meaning for the cases where the excitation energy is of the order of or greater than, the total binding energy of the nucleus.

The contribution due to fission for these calculations has been studied by Dostrovsky et al.[34] and by Pate and Poskanzer.[40] However, fission, as generally defined, should not occur with niobium, and therefore will not be considered.

D. Comparison of the Cascade-Evaporation Model with Experimental Data

A detailed comparison between the Monte Carlo calculations and previously published experimental results is outside of the scope of this discussion. However, it is instructive to mention a few of the gross features. Additional mention of the agreement is presented as it becomes pertinent to the later discussion of the present results.

The agreement of the Metropolis et al. cascade calculations at low energies with published results ranges from satisfactory to good. Their calculations of the production, angular distribution, and kinetic-energy distribution of fast protons are in good agreement with emulsion data.[24] The emission of protons and neutrons, as measured by counters, compares favorably with the prediction of the calculation.[24] When a crude estimation of the evaporation step is included, the mass-yield curve for copper is satisfactorily predicted.[41] However, the under-

estimation of the simple reaction of the type (p,pn) and (p,2p) has been noted by several authors.[42,43] This disagreement is generally attributed to the nonrealistic nuclear square-well potential used in the cascade calculation.

At higher energies (> 400 MeV), the agreement is not as satisfactory. The comparison with emulsion studies show only a qualitative agreement.[25] The mass-yield curve, predicted for copper with the same crude estimation of the evaporation step, showed an underestimation of the products near the target and an overestimation of products removed some distance from the target.[41] The disagreement for the simple reactions is extended to include the more complex (p,pxn) and (p,2pxn) types.[40,43,44] Metropolis et al. have pointed out that the inclusion of better input information concerning meson production may help to rectify the discrepancies.[24,25]

The addition of the evaporation calculation of Dostrovsky et al.[33-37] to the Metropolis et al. cascade calculation has met with considerable success in predicting the production of light products by evaporation. The agreement seems to be satisfactory for products[35,37] up to Z = 3 or 4, but when the procedure is extended to higher mass products, the calculations underestimate experimental results.[38]

The most prominent discrepancy of the calculations is their inability to explain the production of low mass products with Z > 3. These are the products in the valley between the evaporated particles and their parent nuclei. In an effort to rectify the deficiency of the cascade-evaporation model, new mechanisms have been suggested. They will be discussed in Sec. E.

Although the cascade-evaporation model, as described by the Monte Carlo calculations, does not agree with experimental data in all cases, the general agreement is reasonably good. With the inclusion of better input information a number of the discrepancies might be rectified, although it is doubtful whether the low-mass products could be explained. The cascade-evaporation model is therefore considered to explain the

production of the majority of the products, except those of low mass, and believed to be the dominant mechanism for high-energy reactions.

E. Production of Low-Mass Products: "Fragmentation"

The experimental requirement for an additional mechanism to explain the low-mass products comes from both photographic emulsion studies of reaction "stars" and from radiochemical studies. The emulsion data shows a strong energy dependence for the production of these products. Although this behavior is in agreement with the cascade-evaporation model, it has been noticed that stars with two or more multiply-charged fragments are common and compete with the cases having only one fragment at high energies.[3] These stars would have an extremely low probability in the evaporation mechanism. The energy distribution of the fragments, as measured in emulsions, gives a distribution which, for the most part, agrees with the predictions from evaporation. However, the existence of multiply-charged particles, having energies far greater than predicted as well as having energies less than the Coulomb barrier, can not be explained. The angular dependence of the evaporated particles should show an isotropic distribution in the center of mass, but the distributions observed in the study of emulsions are anisotropic.[3] In fact, as the energy of the incident particle increases, the anisotropy also increases.

More recently, the study of the recoil properties of sodium-24 and magnesium-28 has indicated that their production can not be explained by evaporation.[45] The study of fluorine-18 and sodium-24 produced from high-energy bombardments of various targets led Caretto, Hudis, and Friedlander to state that the evaporation mechanism is not sufficient to explain the experimental cross sections.[46] Whether these products of $Z \approx 11$ are formed by the same mechanism as those of $Z \approx 4$ is not certain. However, they also exhibit steep excitation functions[46-50] and their production has been attributed to a mechanism other than that of the cascade-evaporation model. We therefore refer to all of these

products as "low-mass products" but without the requirement that they all be produced by the same mechanism. For convenience, the term "fragmentation" is used to denote these mechanisms.

Perfilov et al. have analyzed the information in the light of the cascade-evaporation model with the inclusion of the possibility of asymmetrical fission.[3] They point out that even though some of the data can be explained by various parts of the model, no one process or combination of processes of the model can explain all the experimental data. These difficulties in explaining the experimental information of low-mass products has led many authors to advance various hypotheses.

The study of the high-energy interactions of protons with lead prompted Wolfgang, Baker, Caretto, Cumming, Friedlander, and Hudis to propose a fast mechanism in which the production and subsequent absorption of mesons played a prominent role.[47] Since meson production becomes significant above 400 MeV for nucleon-nucleon collisions, it is possible to regard it as an important agent for large energy transfer to the nucleus. In most cases, the meson has a short mean free path due to the large absorption resonance at approximately 200 MeV. It is therefore expected that the meson will be reabsorbed by the nucleus depositing large quantities of excitation energy in a limited area. These local "hot spots" are believed to disrupt the local bonds causing fragments of nuclear matter to be emitted before the excitation energy can be equilibrated throughout the nucleus. Thus the fragments are the product of a fast process dependent upon the production of mesons. This mechanism has been used by Caretto et al. to explain the production of low-mass products from the bombardment of various targets.[46]

However, Crespo has pointed out that the necessity for the production of mesons is not supported by a number of experimental results.[45] Instead, his result from the recoil properties of sodium-24 and magnesium-28 have led him to postulate a fast mechanism in which mesons do not play a significant role. A high-energy particle is considered to originate

a complex cascade which essentially cleaves the nucleus into regions of relatively "cool" nuclear matter. Subsequent bombardment of the cool regions by the cascade particles allows the fragments to emerge with energies from the Coulomb barrier up to the high energies that have been observed for the fragments. In essence, this hypothesis is similar to the proposed mechanism of Glassgold et al. in which the fragments are the result of shock waves originated by the bombarding particles "boring" a hole through the nucleus.[51] The cascade can also be related to the "viscous fluid" which Faissner and Schneider have used to explain the fast fission process they have observed.[52]

Various other mechanisms have been extended which view the projectile as interacting with a cluster of nucleons within the nucleus.[53,54] They would explain the extremely high-energy fragments that have been observed. However Sörensen has pointed out that the observation of fragments at large angles are difficult to explain with this mechanism.[55] Also, it is questionable whether the clusters could survive the large bombarding energies.

In spite of the confusion concerning the production of low-mass products, the conculsion can be reached that the cascade-evaporation model can not explain the experimental data by itself. Whether any of the proposed mechanisms given or a combination of them can explain the data is still subject to question. This question can best be resolved by further study.

F. Summary

This brief summary of high-energy reactions provides a basis for the present investigation. Thus it is hoped that the comparison of the proton results with the predictions of the cascade-evaporation model will serve as an indication of the limitations of the model. Similarly, the comparison of the helium-ion results with the proton results should shed some light upon their relative behavior at high energies and give

an indication of the validity of some of the inherent approximations. Finally, it is hoped that the experimental results from both particles will help formulate a better understanding of the fragmentation process.

II. EXPERIMENTAL PROCEDURE

A. Target Arrangement and Irradiation

The irradiations were conducted in the internal beam of the 184-inch synchrocyclotron at the Lawrence Radiation Laboratory. The internal beam current of this machine fluctuates by factors of 2 to 5 on day to day operating conditions. Generally, beam currents of approximately 0.4 microamperes for proton bombardments and approximately 0.10 microampers for helium-ion bombardments were obtained as determined by aluminum monitors. These monitors, discussed below, made it possible to obtain an accurate measurement of the beam current irrespective of any fluctuations.

The practical limits on the energy range of the accelerator are 240 to 720 MeV for protons and 320 to 880 MeV for helium ions.[56] The beam intensity falls off rapidly if the bombarding energy is extended beyond these limits. Although the beam spread is unknown, it is believed that the uncertainty in energy[57] is roughly ± 10 MeV. Since the accelerator focuses the beam by its magnetic field, protons and helium ions are differentiated by their relative charge to mass ratio. However, deuterons and helium ions have the same ratio and consequently will be accelerated under almost identical conditions. This fact raises some question concerning the deuteron contamination to the helium-ion beam. This contamination is believed to become small when the time lapse between deuteron and helium-ion bombardments is of the order of hours and should become negligible when the helium-ion and deuteron bombardments are separated by a time lapse of days.[57,58] The deuteron beam was rarely used during the time of this study. In addition, the helium-ion irradiations were generally conducted after the accelerator had been changed over from protons to helium ions by another experimental group. Consequently, several hours of running time with a helium-ion beam generally preceded the bombardments. Even in the few cases when the accelarator was scheduled for helium-ion bombardments immediately after

deuterons had been used, no noticeable differences were observed in the measured cross sections. Thus, it is felt that the question of deuteron contamination to the helium ion beam does not effect the results of this study.

The accelerator beam was monitored by the sodium-24 production in aluminum. Typically 10.7 mb has been used for the Al^{27} (p,3pn)Na^{24} cross section from about 340 MeV to 6 BeV.[41,45] However, recent measurements of this excitation function by Cumming have led Porile to use the values of 11.0 mb at 0.5 BeV, 0.5 mb at 1.5 BeV, and 9.0 mb at 2.9 BeV.[44] Until these measurements are completed, a comparison between the two excitation functions can not be made here. Greater uncertainty is connected with the Al^{27} (He^4, He^4 pn)Na^{24} cross section for the energy range of 320 to 880 MeV. The excitation function has only been measured to 380 MeV.[59,60] Although the slope of the function decreases slowly, extrapolation might cause serious errors. However, previous workers have assumed a constant value of 24 mb for this energy range[45] due to a lack of better values. Since these uncertainties exist in the monitor cross sections, the ratio of the measured cross section to that of the monitor will be listed. An estimation of the absolute cross section can then be obtained by multiplying the relative cross sections by the best current value for the monitor. In the cases where the monitor activity was too great to obtain accurate values for the sodium-24 count rate, the sodium-24 was allowed to decay, and the sodium-22 activity was counted and corrected to a sodium-24 count rate. These corrections were obtained experimentally by determining the sodium-24 to sodium-22 activity in the aluminum foils as a function of bombarding particle and energy. The ratio of the sodium-24 to sodium-22 activity, corrected for absolute production, is plotted in Fig. 1.

The target arrangement consisted of foils stacked and clamped together by a copper "clothes-pin" target holder as shown in Fig. 2. The foils of niobium and aluminum were cut to dimensions 2 by 3.5 cm and milled as a stack on all sides to insure uniform area. Special care

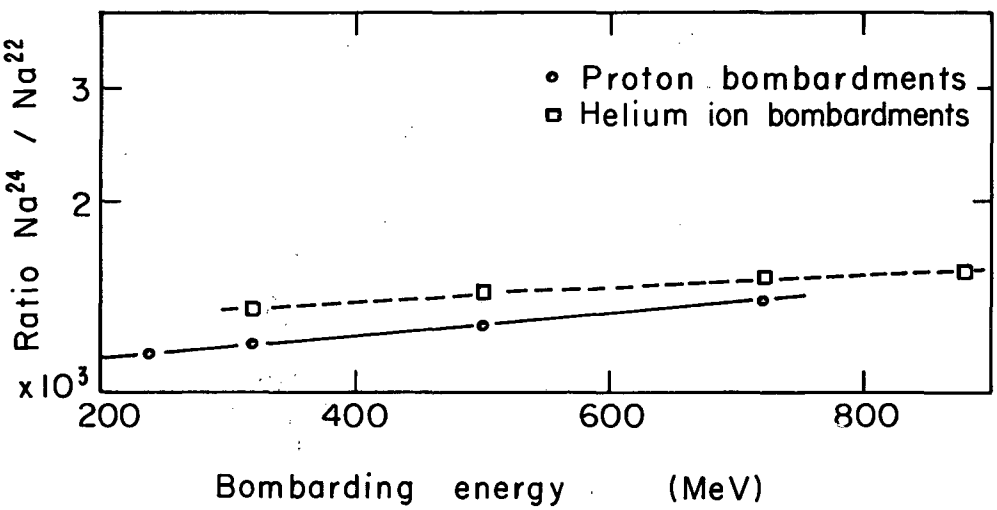

Fig. 1. Ratio of sodium-24 to sodium-22 activity as a function of bombarding energy.

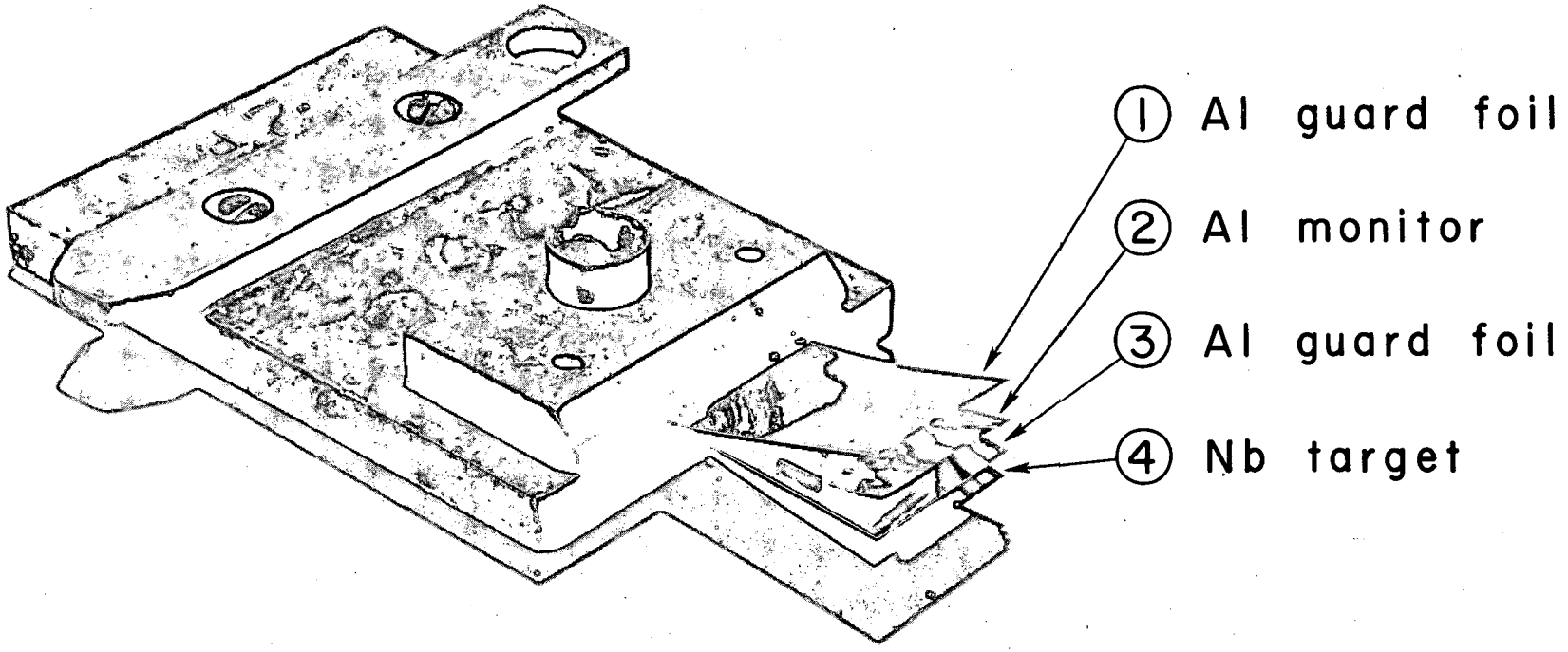

Fig. 2. Target holder and foils.

was taken to maintain clean surfaces and careful alignment in making the target. Since the beam cuts a circular path outward, the alignment of the leading edge of the foil stack is most critical and was therefore machined after the target was made. These precautions insured a uniform beam density on all foils of the irradiated stack. When measurements were conducted to check the uniformity, the error was found to be less than those encountered in mounting and counting the foils. The niobium used in all of the irradiations came from the same 2.5-mil sheet. Spectroanalysis of the niobium sheet gave the impurities listed in Table I. A 1-mil aluminum foil, 99.99% or better, was used for the monitor. Guard foils of 3-mil aluminum were placed on either side of the monitor to give it support and to insure that background sodium-24 resulting from other structural materials of higher Z, did not contiminate the monitor.

Table I. Impurities of the niobium foil.

Imputiry	%	Impurity		%
Oxygen	0.03	Titanium		0.01
Nitrogen	0.03	Tungsten	Less than	0.01
Carbon	0.015	Zirconium	Less than	0.005
Tantalum	0.05	Nickel	Less than	0.005
Iron	0.015			

The actual transportation of the target to and from the synchrocyclotron was performed by the health chemistry group. In addition, it was their responsibility to minitor the radiation for health hazards until the level reached safe limits. Under typical operating conditions, the time from the end of bombardment to the time when chemical separation could be initiated was 10 to 15 min. Under special circumstances, such as short half-lives, the time could be cut down to 5 to 7 min. In the case of long bombardments, where the half-lives of the isotopes under study permitted, the induced target activities were allowed to decay to safe levels.

B. Chemical Procedure

Once the target had been irradiated and chemical separations were to begin, the foils were snipped from the target holder thereby producing a set of irradiated foils of uniform area. After the niobium and aluminum foils were weighed, the niobium foil was placed in a cellulose-nitrate tube for dissolution, and the aluminum monitor foil was stored for later mounting and counting.

The niobium foil was always dissolved with concentrated hydrofluoric and nitric acids. Since fluoride ions dissolve the silicates in glass, it was necessary to precipitate the flouride ions from the traget solution before glass equipment could be used. The general procedure was to add a concentrated solution of calcium nitrate to form calcium fluoride. However, calcium fluoride is slightly soluble in acidic solutions, and therefore, the remainder of the fluoride-ion concentration was precipitated by the addition of concentrated solutions of zirconium and barium nitrate forming barium fluorozirconate. Once the target solution was in this form, it could be transferred to glass equipment.

Inactive carriers of the elements to be separated were added to the initial target solution. They are required for two reasons: First, the maximum amount of any element, other than the target material, that is produced in the irradiations is on the order of 10^{9} atoms (10^{-14} moles). Therefore a quantity of the element must be introduced so that standard analytical procedures can be used and a final precipitate with the mass required for mounting and counting can be obtained. Second, the activity lost in the chemical separations is estimated from the chemical yield. Therefore, a known measurable quantity of the element must be introduced in the initial chemical step. These requirements necessitate conditions suitable for complete exchange between the radioactive and inactive species present in the target solution. These conditions are met by the initial target solutions mentioned above.

Inactive carriers can also be used for increasing the radioactive purity of the chemical separations. If a solution contains activities from different elements, the addition of an inactive carrier will decrease the relative number of active to inactive atoms of that carrier element; Upon subsequent precipitation of the element, a greater percentage of the activity will be removed from solution than if the carrier had not been added. Thus it is possible to reduce the quantity of undesired activities in the solution which would result in a greater degree of radioactive purity. This procedure was used extensively and will be referred to as a "scavenge". A similar procedure, in which an inactive carrier is added to dilute an undesired activity so as to hinder its co-precipitation with the desired activity, was also used to increase the radioactive purity of the samples. These carriers will be referred to as "hold-backs".

The degree of radioactive purity required in the chemical separations depends upon the activity of the isotope to be measured relative to the other activities present in the sample. Thus if the relative cross section and counting efficiency for an isotope are large in comparison to the other activities, the requirements for purity need not be so stringent. With the conditions involved in this study, the chemical separations of copper, nickel, and sodium required a radioactive purification factor of up to 10^7, whereas a factor of 10^4 was permissible for the separations of niobium and zirconium. As far as can be determined from the purity of the gamma-spectra and beta-decay curves for the samples, these factors were obtained by the chemical separations given below. The chemical separations are taken from standard radiochemical procedures with a few changes to adapt them to our requirements.[61,62] For the cases where more then one element was separated per bombardment, a suitable combination of the chemical steps was made.

1. Niobium

Following the elimination of fluoride ions, niobium pentoxide was precipitated from the acidic target soluton by digesting with potassium bromate in a water bath. The oxide was washed with a solution of dilute

nitric acid and ammonium hydroxide, transferred to a cellulose-nitrate tube and dissolved in concentrated hydrofluoric acid. After a barium-fluorozirconate scavenge, niobium pentoxide was precipitated with concentrated ammonium hydroxide, washed with a dilute solution of ammonium and sodium hydroxides, and dissolved by digesting with nitric and oxalic acids. A second acid precipitation of niobium pentoxide was carried out on an aliquot of the solution by heating it after the addition of potassium bromate. The size of the aliquot was determined by the desired weight of precipitate for mounting and counting. The niobium pentoxide was filtered through a weighed paper filter and washed with water, alcohol, and acetone. The sample was weighed and mounted in this form. After counting the sample, the precipitate was ignited to determine the chemical yield. The procedure took approximately 40 minutes.

2. Zirconium

Twenty mg of zirconium carrier was added to the initial target solution. Addition of barium ion caused the precipitation of barium fluorozirconate which was washed with water and dissolved with the addition of concentrated nitric acid and 5% boric-acid solution. The barium ion was eliminated by the addition of sulfuric acid. Zirconium hydroxide was formed by addition of ammonium hydroxide, and, after washing the precipitate with water, it was dissolved in concentrated hydrochloric acid. The solution was adjusted to 6-N hydrochloric acid and extracted with 0.4-M TTA in benzene. The organic phase was washed three times with 1-M nitric acid and back-extracted with 4-N hydrofluoric acid. The first part of the procedure was repeated up to the TTA extraction step. An aliquot of the solution was then precipitated by digesting with 16% mandelic acid. The zirconium tetramandelate was washed with hot water and filtered through a tared glass filter and again washed with water, alcohol, and ether. After drying for 10 min. at 110°C, the sample was weighed and mounted. The chemical separation took about 1.5 hours.

3. Copper

Fifty mg of copper carrier and a number of hold-backs in the region of copper and niobium were added to the dissolved target. The fluoride ion was removed by the standard method. Upon addition of an excess of ammonium hydroxide, the copper remained in solution as the ammonium complex while the niobium, and many other elements, precipitated as the hydroxide. The solution was adjusted to 2-N hydrochloric acid and a sulfide precipitation was carried out. Concentrated hydrochloric and nitric acids dissolved the sulfide, and the addition of sodium sulfite reduced the copper to the plus-one state. Addition of potassium thiocyanate precipitated the cuprous thiocyanate which was dissolved with concentrated hydrochloric and nitric acids. Niobium, zirconium, yttrium, and iron ions were added for a hydroxyl scavenge. The copper was then reduced to the metallic form by sodium hydrosulfite in a strongly basic solution. The metallic copper was dissolved in nitric acid, and the procedure was repeated from the thiocyanate precipitation. The copper was filtered through a weighed glass filter, washed with water and acetone, weighed, and mounted. Approximately 45 minutes were required for the separation.

4. Nickel

Ten mg of nickel carrier together with a number of hold-back carriers in the region of niobium were added to the target solution. Following the elimination of the fluoride ion, an excess of ammonium hydroxide was added to precipitate the niobium and a number of the other hydroxides, leaving nickel in solution in the form of the ammonium complex. A copper-sulfide precipitation was followed by a niobium, zirconium, yttrium, and iron hydroxyl scavenge. The nickel was then precipitated with 1% dimenthylglyoxime and redissolved in hydrochloric acid. A second copper sulfide precipitation succeeded by a dimethylglyoxime precipitation yielded a sample free from contamination. The precipitate was filtered through a tared glass filter and washed with water. After drying for 10 minutes at 110°C, the sample was weighed and mounted. The procedure took about one hour.

5. Sodium

Twenty mg of sodium carrier were added to the dissolved target, and the fluoride ion was eliminated. Addition of ammonium hydroxide precipitated the niobium. Copper was added to the supernate to precipitate cupric hydroxide as a scavenge. Iron hydroxide was then precipitated for the same purpose. The solution was evaporated nearly to dryness and 6-M ammonium acetate was added. Sodium was precipitated by stirring with a solution of uranyl acetate, magnesium acetate, and acetic acid, and washed with a solution of glacial acetic acid, anhydrous ethyl acetate, and anhydrous ethanol. The precipitate was suspended in n-butanol. N-butanol saturated with dry hydrogen chloride was added to change the precipitate to sodium chloride which was washed with a solution of n-butanol and n-butanol saturated with hydrogen chloride. The sodium precipitation was repeated, and the organic material was expelled by heating. A small amount of potassium ion was added together with perchloric acid, and the solution fumed to dryness. N-butanol was added and the mixture was boiled to dissolve the sodium perchlorate. Sodium chloride was again precipitated from the supernate by addition of n-butanol saturated with hydrogen chloride. The precipitate was filtered through a tared glass filter, washed with n-butanol, dryed for 10 minutes at 110° C, weighed, and mounted. The separation took approximately 3.5 hours.

The samples were always mounted in the same manner. A chimney arrangement of 1.9-cm diam. was used in conjunction with a sintered glass disk and vacuum filtration. Either a paper or glass filter was used to filter the precipitate depending upon whether the precipitate required ignition to determine the chemical yield. This filter (2.1-cm diam.) was mounted on aluminum cards (50 mils, $\approx$ 350 mg/cm^2) by means of double-edge Scotch tape. A 0.1-mil (0.5 mg/cm^2) film of rubber hydrochloride was then affixed over the sample by the same tape which mounted and overlapped the sample. This procedure gave samples which were stable to normal handling for long periods of time. In general, approximately 8 mg/cm^2 samples were made so that a uniform precipitate could be obtained, but under individual circumstances this weight was changed to meet the specific requirements.

The errors in the chemical procedure involved those of weighing the foils and determining the chemical yield. These errors are estimated to be within 5%.

C. Procedure for Measurement of Radioactivity

Quantitative measurement of the induced activity was almost exclusively determined by measurement of the beta-radiation of the radioactive isotopes under study. Initially, it was hoped that the gamma-radiation could also be used for quantitative measurement. However, it was found that the complexity of the gamma-spectrum rendered the tool ineffective from the viewpoint of both accuracy and time involved in analyzing the spectra. The gamma-spectra were therefore used, for the most part, in identification of the radioactive isotopes present in the samples.

The counters used in measuring the beta-activity were methane-flow, end-window, proportional counters. The design has been developed at this laboratory to the point where they are stable to within a fluctuation of 1% over a period of six months to a year as determined by daily counting of a uranium-metal standard. The criteria for determining whether the counters were operating satisfactorily were: (1) the standard varied no more than 0.5% from the average count rate; (2) the background did not exceed 9 counts per minute. The average background was 7.5 to 8.5 counts per minute with daily fluctuations of 0.25 to 0.50 counts per minute. Gentle variations of the average daily background were noticed over extended periods of time.

These counters were standarized for absolute counting, in cooperation with Blann,[63] by a procedure reported by Bayhurst and Prestwood.[64] An experimental relationship between the counting efficiencies of the counters and the average beta energy was employed rather than correcting for self-absorption, backscattering, etc., independently. Initially, the counting efficiencies of a set of beta emitters were

determined as a function of beta energy and mass of sample. The absolute disintegration rate of the samples were obtained from 4π counting measurements. From a plot of this data and the relationships between average energy and end-point energy as given by Bayhurst and Prestwood, it was possible to construct a plot of counting efficiency versus the average energy of the beta particle for varying sample masses. Once a series of these plots was made, it was possible to obtain the counting efficiency of any other beta emitter.

The authors have stated the possibility of determining the counting efficiency to within 3% by this method, but it is believed that for our standardization only 5 to 10% accuracy could be claimed. However, in the determination of cross sections, the fact that they were determined relative to the beam monitor decreases the errors. Thus, it is possible to expect errors of less than 5% due to the counting efficiencies of the beta emitters.

Gamma-radiation was measured by a 3 by 3-in. sodium-iodide crystal mounted on a photomultiplier and used in conjunction with a 100—channel analyser. The analyser could be energy-calibrated by measurement of suitable standards of known energy and was therefore a powerful tool for identification of activities, both desired and undesired. A quantitative measurement could be made by a "peak-stripping" procedure. Standard pure gamma-spectra were used to estimate the contribution of a gamma to the rest of the spectrum. This standard spectrum was then subtracted from the rest of the original spectrum leaving a new one without the first gamma's contribution. Starting with the highest energy gamma, successive peaks were subtracted until the desired peak was reached. Then a quantitative measurement could be made with the aid of Health's values for absolute gamma counting.[65] However, as mentioned earlier, with increased complexity of the spectrum the procedure becomes increasingly difficult and inaccurate.

Generally, statistics of better than 1% were obtained for the beta counting with errors due to timing less than 0.25%. Thus, including the

fluctuations in positioning the samples, the counting errors were less than 2%. If the counting rate dropped to the order of 20 counts per minute, the counting errors increased to 5 or 10% due to fluctuations in the background. However, the increased errors were minimized by the fact that the half-lives involved in these cases were long enough to permit a number of determinations of the counting rate, and a statistical average could be obtained. A standard error of 3% was attributed to the graphical analysis of the beta-curves. In some of the more complex curves, a least-squares fit to the data was obtained by a program on the IBM 704 computer.[66] Also, use was made of the Biller plot[67] for cases of two pure activities of comparable half-lives. The errors in counting efficiencies are within 5%, but decay-scheme corrections can constitute a source for large errors in absolute determinations. The values[68,69] used in this work are listed in Table II. In general, it is believed that the combination of decay-scheme corrections and counting-efficiency errors is about 10%. Although some of the measured cross sections can have large absolute errors, the relative errors for an isotope are minimized since all the values for a specific isotope were obtained in a similar way. Thus, only the bombardment, chemical, counting, and decay-curve analysis errors are involved. In general, a 10% error is quite liberal for these relative cross sections.

Table II. Decay Systematics.

Isotope	t	Rad.	Energy (MeV)	%	Isotope	t	Rad.	Energy (MeV)	%
Nb-90	14.7 h	β^+	1.50	50	Cu-64	12.88h	β^-	0.573	38
		e^-	0.114	11			β^+	0.656	19
		e^-	0.123	19	Cu-61	3.32h	β^+	0.56	3
Nb-89	1.79h	β^+	2.86	91			β^+	0.94	5
							β^+	1.15	1.1
Zr-89	79.3 h	β^+	0.90	30			β^+	1.21	53.1
		γ	0.915	100					
					Ni-66	54.8 h	β^-	0.20	100
Sr-87m	2.75h	e^-	0.363	22					
					Cu-66	5.10m	β^-	1.59	9
Zr-88	85 d	γ	0.394	100			β^-	2.63	91
		e^-	0.377	4.62					
					Ni-65	2.56h	β^-	0.60	23
Y-88	105 d	β^+	0.57	0.7			β^-	1.01	8
							β^-	2.10	69
Zr-87	1.57h	β^+	2.10	83					
					Ni-57	36 h	β^+	0.849	39.9
Zr-86	17 h	γ	0.241	100			β^+	0.712	5.6
Y-86	14.6 h	β^+	0.90	3	Na-24	15 h	β^-	1.391	100
		β^+	1.32	15					
		β^+	1.41	5	Na-22	2.58y	β^+	0.544	89.8
		β^+	2.09	6					
Y-87m	14 h	e^-	0.363	22					
Cu-67	61.6 h	β^-	0.395	45					
		β^-	0.484	35					
		β^-	0.577	20					
		e^-	0.083	$\approx$20					

III. EXPERIMENTAL RESULTS

A. Measurement of Cross Section

Once the activity of an isotope was determined, its disintegration rate was calculated by

$$D = \frac{(A)\ (C)}{(\epsilon)} \qquad \text{(III-1)}$$

where D is the isotope's disintegration rate at the end of bombardment, A is its activity at the end of bombardment, ϵ is its counting efficiency, and C is its chemical yield. From the disintegration rate of the isotope and the aluminum monitor, the ratio of the cross section for the production of the isotope from niobium to that of the sodium-24 from aluminum was calculated by

$$\frac{\sigma}{\sigma_{Na}} \frac{D\ W_{A\ell} M_{Nb} (1 - \exp - \lambda_{Na} t)}{D_{Na} W_{Nb} M_{A\ell} (1 - \exp - \lambda\ t)}, \qquad \text{(III-2)}$$

where σ and σ_{Na} are the cross sections for the isotope and the monitor, W_{Nb} and $W_{A\ell}$ are the weights of the foils in grams, M_{Nb} and $M_{A\ell}$ are the molecular weights of the foil materials, and t is the length of bombardment. In the cases where the half-lives of the measured isotopes were long in comparison to the bombardment time, the factor $\frac{(1 - \exp - \lambda_{Na} t)}{(1 - \exp - \lambda\ t)}$ was expressed by its first term $\frac{\lambda_{Na} t}{\lambda\ t}$ or $\frac{t_{1/2}}{t_{1/2,Na}}$, where $t_{1/2}$ is the half-life of the isotope.

The experimental results for the proton and helium-ion bombardments are listed in Tables III and IV in blocks according to bombarding energy. In all cases, the ratio of the cross section for the isotope to that for the aluminum monitor is given. Each block contains the average value of the determined ratios under $\bar{X}$, the standard error of these values under $\sigma_{\bar{x}}$, and the number of determinations under D. The

Table III. Relative cross sections from proton bombardments of niobium targets.

240-MeV Protons on Niobium				320-MeV Protons on Niobium		
$\bar{X}$	$\sigma_{\bar{X}}$	D	Isotope	$\bar{X}$	$\sigma_{\bar{X}}$	D
6.90		1	Nb-90	5.17	0.50	2
2.63		1	Nb-89	2.05		1
6.60	2.5×10^{-2}	2	Zr-89	5.63		1
8.52		1	Zr-88	6.76		1
4.92		1	Zr-87	4.00		1
1.54×10^{-4}	4.5×10^{-6}	2	Cu-67	4.91×10^{-4}	2.5×10^{-5}	2
2.20×10^{-3}	1.5×10^{-4}	2	Cu-64	9.75×10^{-3}	2.6×10^{-4}	2
5.45×10^{-4}	6.2×10^{-5}	2	Cu-61	3.23×10^{-3}	1.4×10^{-4}	2
1.08×10^{-5}		1	Ni-66	3.58×10^{-5}		1
5.79×10^{-5}		1	Ni-65	2.97×10^{-4}		1
3.67×10^{-5}		1	Ni-57	1.67×10^{-4}		1
8.64×10^{-4}		1	Na-24	1.40×10^{-3}	4.0×10^{-5}	2
2.04×10^{-3}	1.3×10^{-4}	2	Na-22	1.50×10^{-3}	1.9×10^{-4}	2

500-MeV Protons on Niobium				720-MeV Protons on Niobium		
$\bar{X}$	$\sigma_{\bar{X}}$	D	Isotope	$\bar{X}$	$\sigma_{\bar{X}}$	D
4.47	0.24	2	Nb-90	3.49	0.35	2
1.67		1	Nb-89	1.31		1
4.23	2.5×10^{-2}	2	Zr-89	3.63		1
5.11		1	Zr-88	3.97		1
3.09		1	Zr-87	2.46		1
2.77×10^{-3}	1.6×10^{-5}	2	Cu-67	1.12×10^{-2}	4.7×10^{-4}	3
6.90×10^{-2}	3.4×10^{-3}	2	Cu-64	0.263	1.3×10^{-2}	3
3.92×10^{-2}	3.5×10^{-3}	2	Cu-61	0.163	1.0×10^{-2}	3
2.70×10^{-4}	3.5×10^{-6}	2	Ni-66	7.83×10^{-4}	1.5×10^{-5}	2
2.08×10^{-3}	1.3×10^{-4}	2	Ni-65	5.92×10^{-3}	1.0×10^{-5}	2
1.73×10^{-3}	1.5×10^{-4}	2	Ni-57	6.89×10^{-3}	3.5×10^{-5}	2
4.03×10^{-3}	1.2×10^{-4}	2	Na-24	1.23×10^{-2}	1.0×10^{-4}	2
2.42×10^{-3}	1.0×10^{-4}	2	Na-22	6.88×10^{-3}	9.0×10^{-5}	2

Table IV. Relative cross sections from helium-ion bombardments of niobium targets.

320-MeV Helium ions on Niobium				500-MeV Helium ions on Niobium		
$\bar{X}$	$\sigma_{\bar{x}}$	D	Isotope	$\bar{X}$	$\sigma_{\bar{x}}$	D
5.37	0.27	2	Nb-90	4.05	0.31	2
1.95		1	Nb-89	1.48		1
4.61		1	Zr-89	3.39	3.0×10^{-2}	2
6.04		1	Zr-88	4.38		1
3.84		1	Zr-87	2.74		1
4.49×10^{-4}	1.0×10^{-5}	3	Cu-67	2.98×10^{-3}	1.6×10^{-4}	3
7.19×10^{-3}	8.3×10^{-4}	3	Cu-64	6.05×10^{-2}	1.7×10^{-3}	3
1.84×10^{-3}	7.0×10^{-5}	3	Cu-61	2.71×10^{-2}	1.0×10^{-3}	3
4.40×10^{-5}		1	Ni-66	3.04×10^{-4}		1
2.53×10^{-4}		1	Ni-65	1.70×10^{-3}		1
2.25×10^{-4}		1	Ni-57	1.50×10^{-3}		1
1.80×10^{-3}		1	Na-24	4.70×10^{-3}		1
1.95×10^{-3}		1	Na-22	3.60×10^{-3}		1

720-MeV Helium ions on Niobium				880-MeV Helium ions on Niobium		
$\bar{X}$	$\sigma_{\bar{x}}$	D	Isotope	$\bar{X}$	$\sigma_{\bar{x}}$	D
3.48	0.10	2	Nb-90	3.01	0.15	3
1.16		1	Nb-89	1.13	6.0×10^{-2}	2
3.08		1	Zr-89	2.63		1
3.88		1	Zr-88	3.32		1
2.33		1	Zr-87	1.99		1
6.91×10^{-3}	2.6×10^{-4}	2	Cu-67	1.07×10^{-2}	9.8×10^{-4}	4
0.181	3.5×10^{-3}	2	Cu-64	0.261	9.6×10^{-3}	4
0.108	2.0×10^{-3}	2	Cu-61	0.198	1.4×10^{-2}	4
8.02×10^{-4}		1	Ni-66	1.19×10^{-3}	6.1×10^{-5}	3
5.06×10^{-3}		1	Ni-65	6.97×10^{-3}	4.2×10^{-4}	3
5.96×10^{-3}		1	Ni-57	1.01×10^{-2}	8.3×10^{-4}	3
1.25×10^{-2}		1	Na-24	2.22×10^{-2}		1
8.18×10^{-3}		1	Na-22	1.06×10^{-2}		1

standard error[70] was calculated by

$$\sigma_{\bar{x}} = \left[\frac{1}{n(n-1)} \sum_{i}^{n} (x_i - \bar{x})^2\right]^{1/2}. \qquad \text{(III-3)}$$

where n is the number of determinations, x_i is the measured values, and $\bar{x}$ is the average of the values. For the cases where only one measurement was made, the cross sections are listed under $\bar{X}$, but no standard error value is given. Note that the standard error exceeds 10% of the value for only three cases, indicating that the previously estimated relative uncertainty of 10% is valid.

For some of the isotopes, the yields include contributions from the decay of short-lived isobars. As an example, in the measurement of zirconium-88, it must be assumed that the measured value includes the cross sections for all the nuclei of mass 88 produced with $Z \geq 40$, whereas the measured value of copper-67 must be assumed to include the cross sections for all of mass 67 with $Z \leq 29$. An estimate of these contributions to the measured values is given below.

The results are graphed in Figs. 3 through 7. Error bars are not included because of the uncertainty in absolute errors caused by decay-scheme corrections and because of our desire to eliminate graphical confusion. A discussion of these measurements is given under their respective elements.

1. Niobium

Niobium-89 and 90 were measured by their beta activities. Activities of niobium-91m, 92, and 95 were also observed, but a quantitative measurement was not attempted because of experimental difficulties. Gamma analysis was used only for identification because of the complexity of the spectrum. It is worthwhile to note that niobium-95 was observed in the helium-ion bombardments and not in the proton bombardments. This may be interpreted as evidence for a stripping reaction. A new activity of about 15 minutes half-life was observed and believed to be the unreported niobium-88. This observation will be discussed in greater

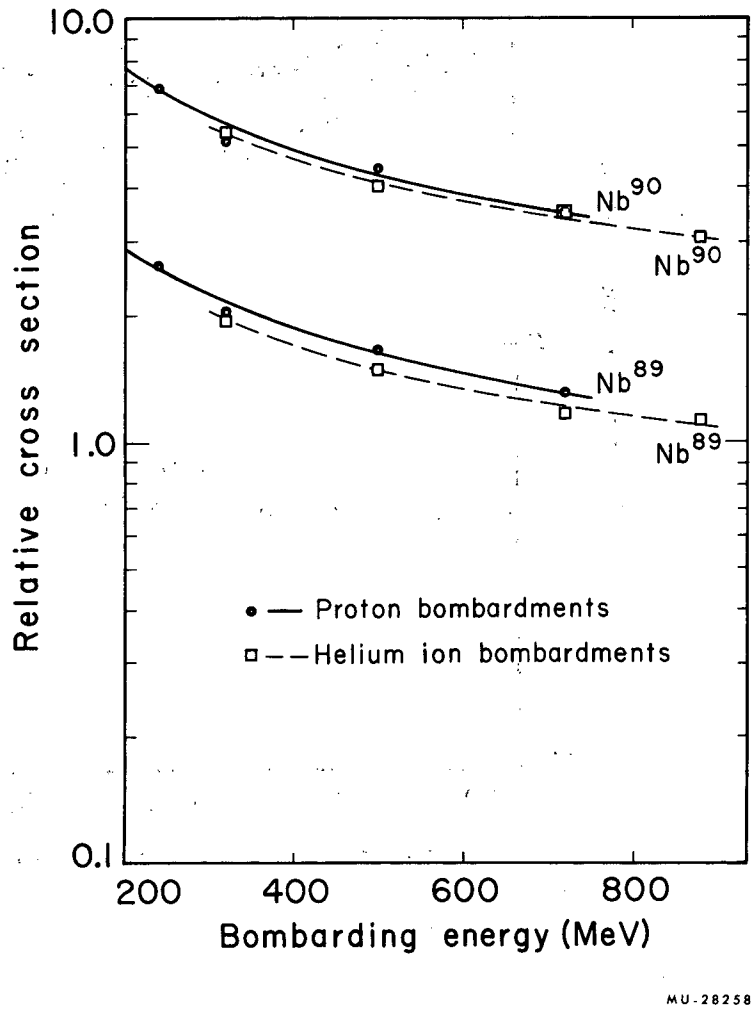

Fig. 3. Excitation functions for the production of niobium isotopes from the bombardment of niobium targets with protons and helium ions.

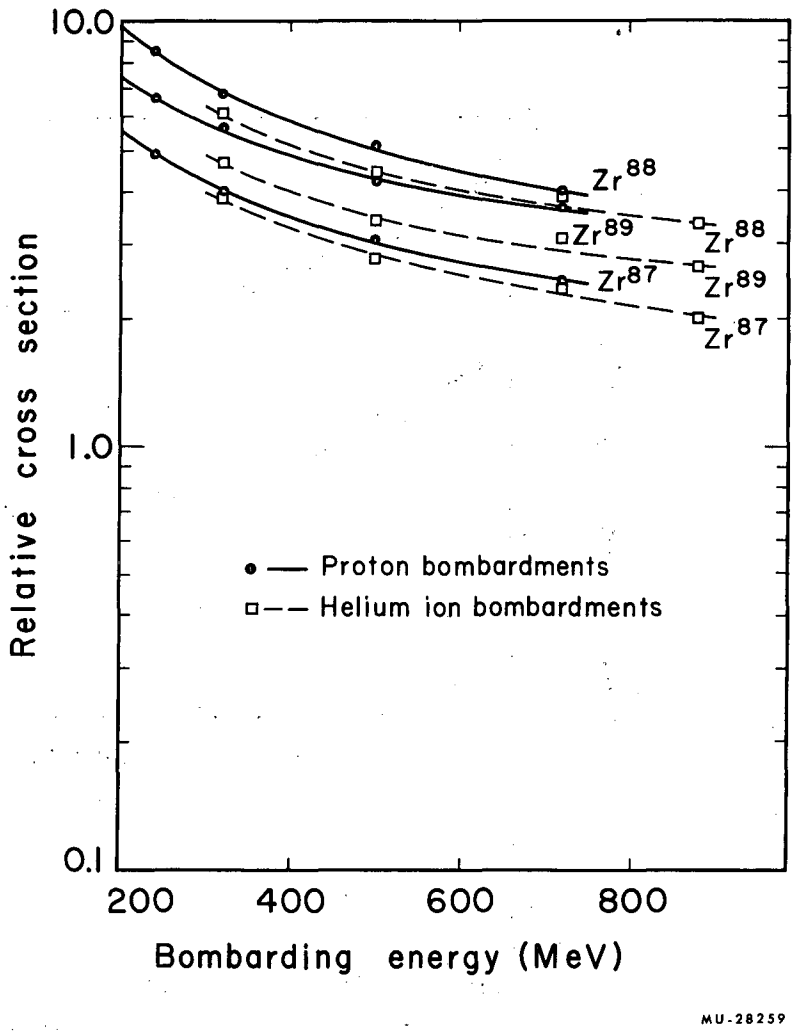

Fig. 4. Excitation functions for the production of zirconium isotopes from the bombardment of niobium targets with protons and helium ions.

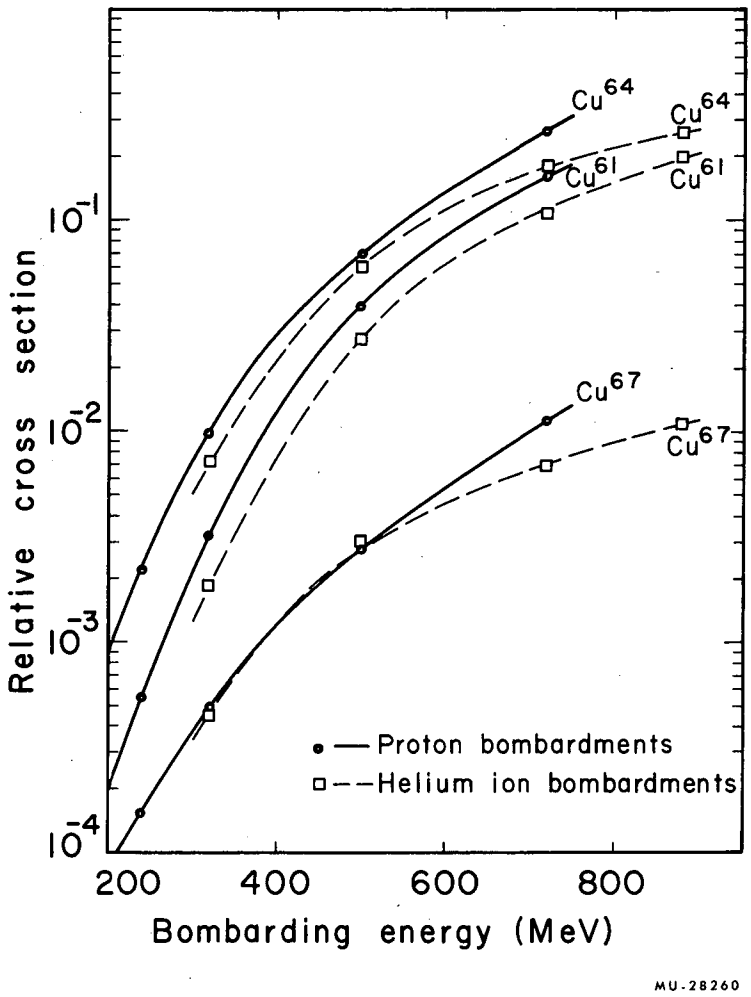

Fig. 5. Excitation functions for the production of copper isotopes from the bombardment of niobium targets with protons and helium ions.

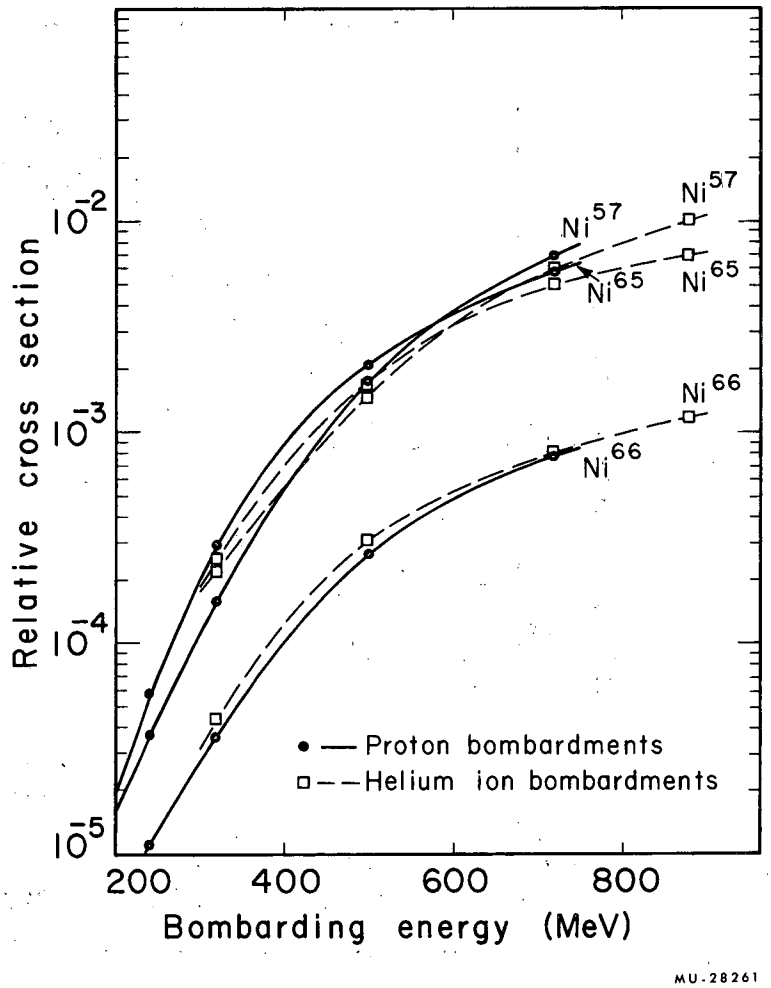

Fig. 6. Excitation functions for the production of nickel isotopes from the bombardment of niobium targets with protons and helium ions.

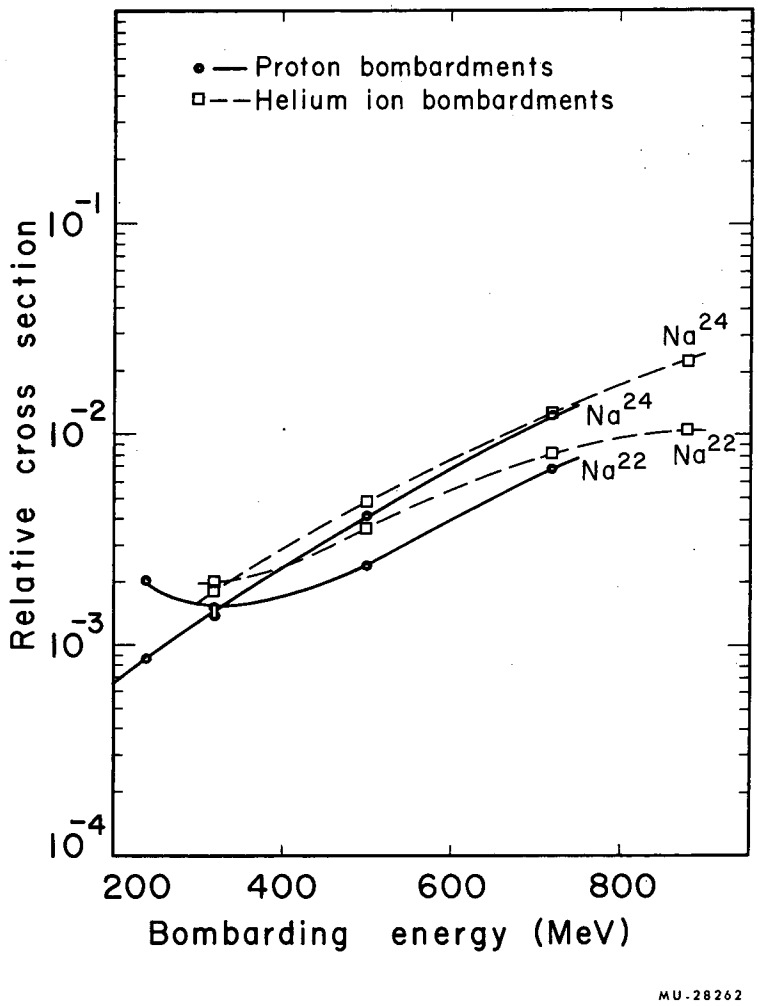

Fig. 7. Excitation functions for the production of sodium isotopes from the bombardment of niobium targets with protons and helium ions.

detail in the next section. Since all of the main photo peaks could be identified with known radiations from the decay of niobium isotopes, and since the prominent zirconium peaks were absent, the samples were considered to be pure. Also, the analysis of the beta-decay curves gave good agreement with the listed half-lives for the isotopes involved and did not include extraneous activity.

The experimentally observed half-life of niobium-89 (1.79 h) was used because of the uncertainty in the decay properties of the isotope.[71,72] It must be assumed that the results for niobium-89 include a contribution from isobars with $Z > 41$, but it is estimated to be quite small ($< 10\%$). The measurement of niobium-90 was complicated by the zirconium-89 growth from the decay of niobium-89. However, by repeating the niobium chemical separation 24 hours after bombardment on an aliquot of the niobium fraction, the niobium-90 could be observed free of the 79.3 hour zirconium. The contribution to the value for niobium-90 from isobars with $Z > 41$ was estimated to be very small ($\leqslant 1\%$) because of the 5.7-hour half-life of molybdenum-90 and because of the relatively low cross section expected for it. Thus, no further errors need be assigned to the niobium results other than those already listed and those in the counting yields.

2. Zirconium

Measurements were made of the zirconium-87, 88, and 89 isotopes. Zirconium-86 decays by electron capture for which the counting yield for beta decay is not known; therefore, it could only be determined through its daughter, yttrium-86, in the beta counters. The yttrium-86 beta activity was in turn buried under the zirconium-89 activity which was made its determination quite inaccurate. The zirconium-86 could also be measured by the 241-keV gamma present in its decay, but the gamma-spectrum analysis became inaccurate when extended to this energy region. Both approaches were attempted initially only to confirm the inaccuracy of the methods.

Zirconium-87 was measured by its activity in the beta-counters as was the zirconium-88 and 89 even though the gamma-spectrum allowed the quantitative measurement of the latter. Zirconium-88 was directly measured by the conversion electrons of the 394 keV gamma which were in turn calibrated by the 394 keV photo peak. Yttrium-87 complicated the measurement of zirconium-89, but by separating a second zirconium sample 24 hours after bombardment from an aliquot of initially pure zirconium, the zirconium-89 could be observed free of the yttrium-87. It must be assumed that the values for zirconium-87 and 88 include a contribution from isobars with $Z > 40$; however, because of our knowledge of the niobium-89 cross section, we attribute less than 20% of these zirconium-87 and of values to the higher isobars. Owing to the 1.79-hour half-life of niobium-89, it was estimated that less than 10% of the niobium-89 decayed into zirconium-89 before chemical separation could be completed. In all cases, the measured half-lives were in agreement with the listed values and no extraneous activity was observed. This observation, with the fact that no photo peaks were seen that could not be attributed to the decay of a zirconium isotope, testifies to the purity of the samples.

A comparison between the values obtained from resolving the gamma-spectrum and the beta-decay curve was conducted at 880 MeV with incident helium ions. The agreement was satisfactory and further time-consuming gamma-spectrum resolutions were terminated. Due to the complexity of the daughter activities in the beta-decay curves, the data was fitted with a least-squares analysis programmed on the IBM 704 computer.[66] Good fits were obtained for all the isotopes except zirconium-86 which still gave a spread, as expected from the preceding discussion. Therefore, the only additional error for the listed results other than those given before and those in the counting yields, is in the uncertainty of Heath's absolute gamma counting values.[65] A comparison was made between beta and gamma counting of sodium-22 under identical experimental con-

ditions. Since the values agreed within 5%, it was felt that no additional errors need be attributed to the measurement of zirconium-88 either.

3. Copper

Copper-61, 64, and 67 were measured by their beta-radiation. It was found that accurate resolution of the 62 and 66 isotopes could not be made due to their similar half-lives and the impurities resulting from the shortened chemical procedure required for the measurement of the 62 and 66 isotopes. However, with the chemical procedure listed above, the copper samples were obtained without noticeable extraneous activity. It is assumed that in the measurement of copper-61 and copper-67, the results included a contribution from isobars with $Z \neq 29$. From a knowledge of the nickel-66 cross section, the contribution to the copper-67 value is believed to be very small ($\lesssim 1\%$). Although the contribution is believed to be larger for copper-61 than copper-67, it can be estimated to be less than 10% of the copper-61 value. Thus, the errors of the copper results include only the listed errors and the counting yield uncertainties.

4. Nickel

Nickel-57, 65, and 66 were the only observed beta-activities in the nickel samples. Although the mass 57 and 66 isotopes have similar half-lives, good resolution was possible with Biller plots.[67] From the behavior of the plots, it is believed that the regular 3% error attributed to the graphical analysis will cover their errors. However, all of the isotopes must be considered to include a contribution from isobars with $Z \neq 28$. From the fact that these isotopes of cobalt and copper are far removed from stability, the contribution can be estimated to be small, especially for nickel-65 and 66. Therefore, the only errors in the values for the nickel isotopes come from the listed errors and the counting yield corrections.

5. Sodium

Pure sodium fractions were obtained as evidenced by the accurate sodium-24 half-life and the almost constant activity of sodium-22. Values for the cross sections were calculated for both isotopes although the counting rate of the sodium-22 was only 1 to 30 counts per minute. The counting errors involved with this count rate are larger because of fluctuations in the background. However, multiple determinations gave an average count rate good to 5% in most cases. One source of error was the possibility that some of the uranium, which was added during the chemical prodecure, managed to follow the sodium and become a sizeable fraction of what was believed to be sodium-22. This question was somewhat resolved by the fact that the cross sections for sodium-22 production were the same whether the count rate was 30 counts per minute or just a few. The values for both isotopes include contributions from isobars with $Z \neq 11$. Whether this contribution is relatively large or small is difficult to estimate, for both the cross sections involved and the mode of production are unknown.

B. Niobium-88

A discrepancy was noted during the course of analyzing the gamma spectra of the niobium samples. In the samples that had been separated immediately after bombardment, a 394-keV photo peak was observed 60 days after bombardment, whereas the peak was absent in the samples which had been reseparated 24 hours after bombardment (see Fig. 8). This observation indicated that the gamma was from the decay of a niobium isotope, but not from any of the reported isotopes except possibly niobium-89. However, the activity from the niobium-89 daughters should have been reduced by a factor of 10^6 by this time, and therefore, the photo peak could not be from the decay chain of the 89 isotope. Also an unassigned beta activity, of about 15-minute half-life, was observed in the initially separated niobium samples. The one isotope which would explain this

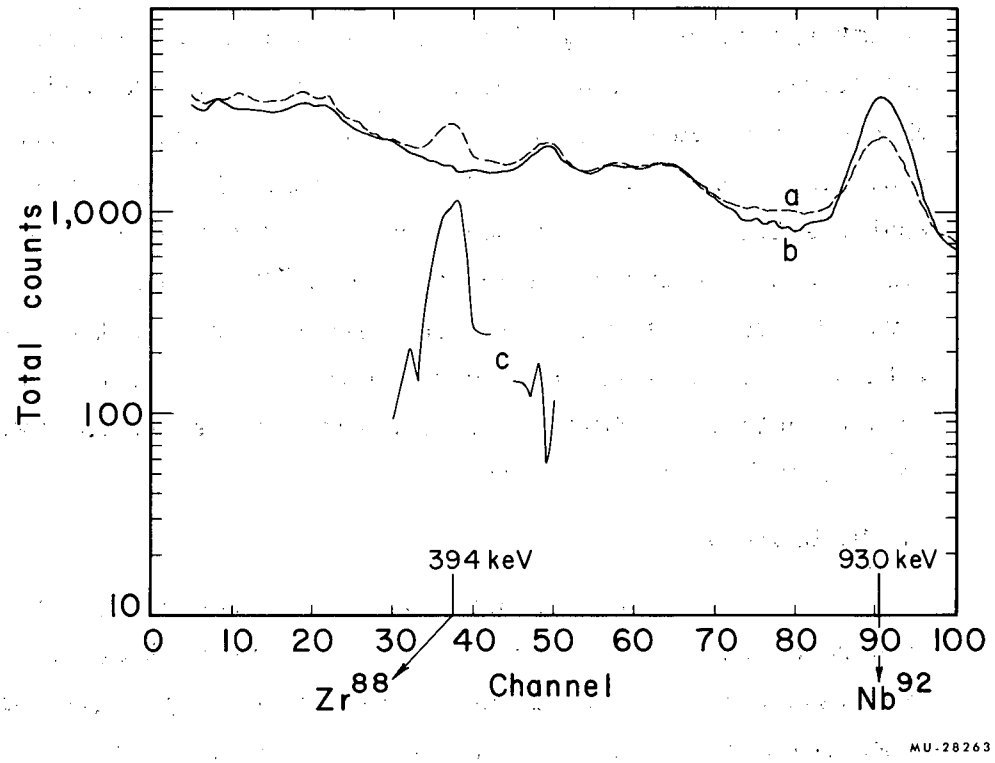

Fig. 8. Gamma-spectra of niobium samples:
(a) Niobium sample separated immediately after bombardment.
(b) Niobium sample separated 24 hours after bombardment.
(c) 294 keV photo peak obtained by subtracting spectrum (b) from (a).

information was the unreported niobium-88. If the beta-activity was due to the postulated isotope, it would indicate a short half-life isotope feeding its daughter zirconium-88, which in turn would explain the 394-keV photo peak by its decay.

Proof that the 394-keV photo peak was due to the decay of a zirconium isotope was obtained by conducting a zirconium separation on a fraction of the initially pure niobium which had been separated immediately after bombardment. The 394-keV photo peak appeared in the zirconium fraction while the 930-keV photo peak of niobium-92 remained in the niobium fraction. (See Figs. 9 and 10.) Since these test cases were from a proton bombardment and because the time lapse from bombardment was greater than 60 days, we established that the 394-keV photo peak derived from the decay of zirconium-88.

We decided to augment this information by producing the isotope by reactions induced with complex nuclear particles. Siver foils (1/10 mil, $\approx$ 2.4mg/cm^2) were allowed to stand overnight in bromine and thereby form uniform targets of pure silver bromide ($\approx$ 4.2 mg/cm^2). These were bombarded with accelerated carbon nuclei in the heavy-ion linear accelerator at this laboratory. A shortened niobium separation was performed, and the samples were counted on both the beta and gamma counters. The time lapse from the end of bombardment to the initiation of activity measurements was 43 minutes.

The beta curve gave an enhanced 15-minute component to the otherwise standard beta curves (See Fig. 11). The gamma analysis gave a number of photo peaks which decayed rapidly, some of which are listed with their measured half-lives in Table V. Typical gamma-spectra are given in Fig. 12. A repeat of the experiment yielded the same results.

It was concluded, from this information, that the previously unreported niobium-88 isotope had been seen with an approximate 15-minute half-life.

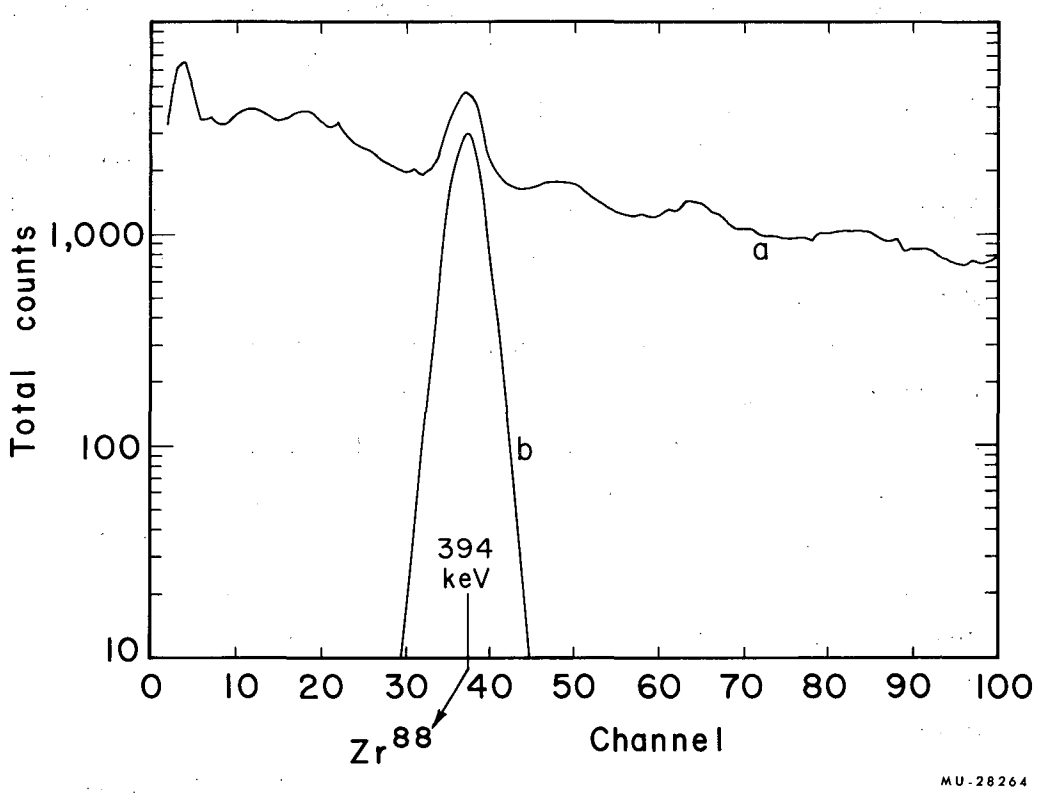

Fig. 9. Gamma-spectrum of zirconium fraction:
(a) Gross spectrum.
(b) 394 keV photo peak obtained by subtracting background from the gross spectrum.

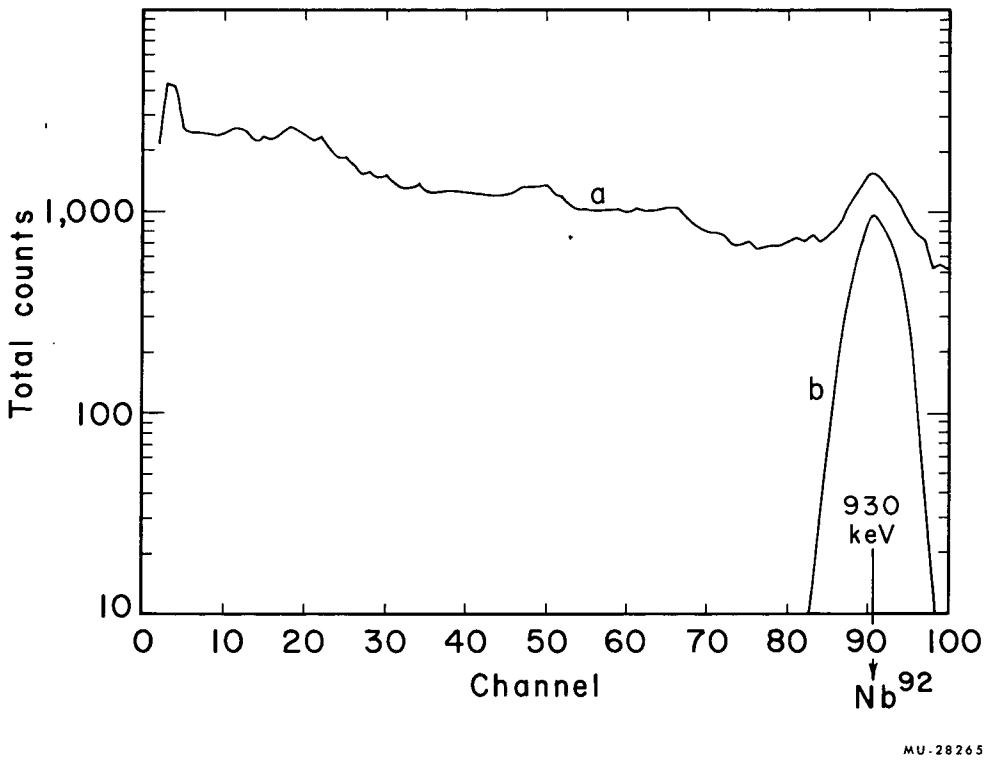

Fig. 10. Gamma-spectrum of niobium fraction:
(a) Gross spectrum.
(b) 930 keV niobium-92 photo peak obtained by subtracting background from the gross spectrum.

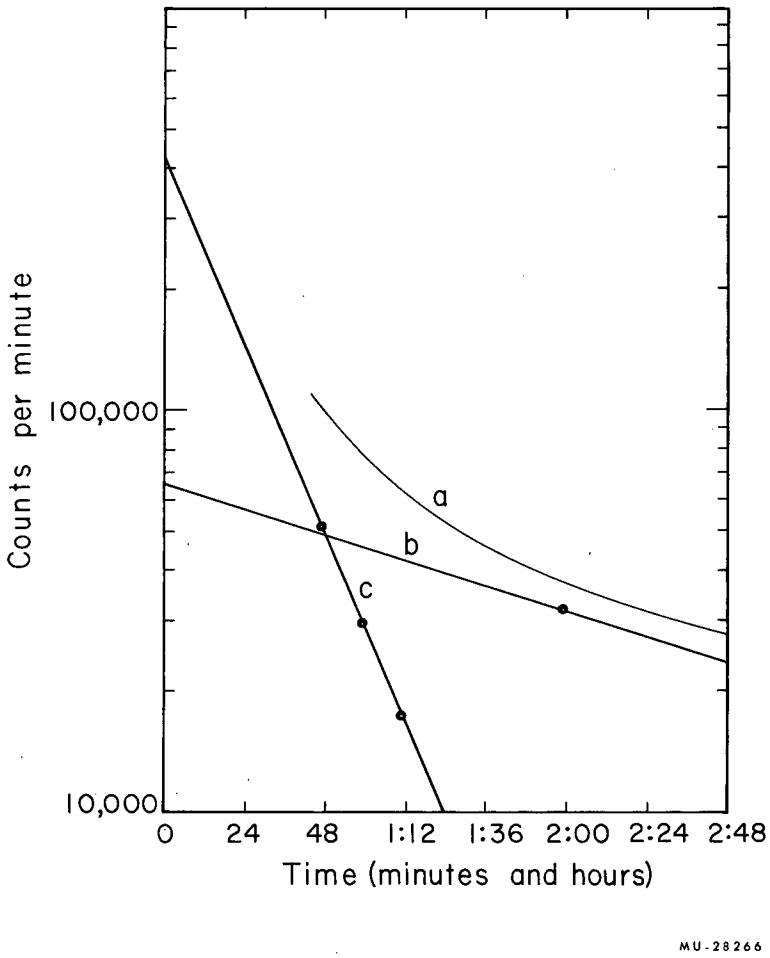

Fig. 11. Beta-decay curve of niobium sample:
(a) Gross curve.
(b) Niobium-89 component.
(c) 15 minute half-life component believed to be niobium-88.

Table V. Observed short half-lived gamma in the niobium sample.

Energy (MeV)	t (min)
0.080	14
0.275	17
0.395	13
1.04	20
0.66	15

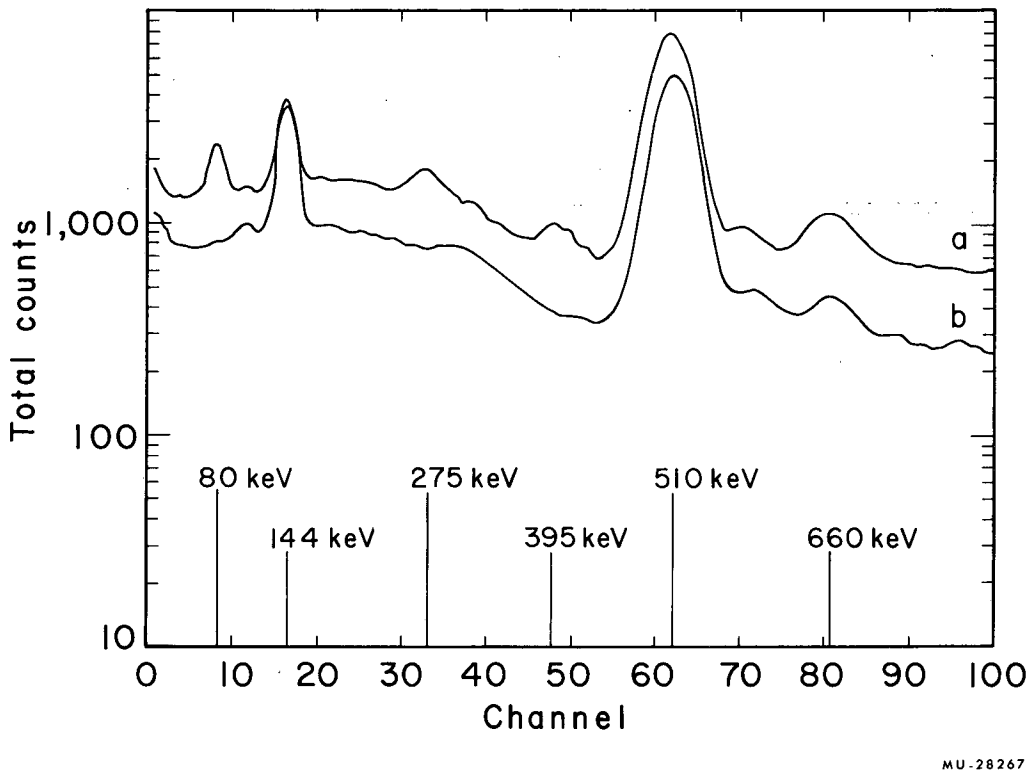

Fig. 12. Gamma-spectra of niobium samples from HILAC bombardment:
(a) Spectrum 29 minutes after bombardment.
(b) Spectrum 115 minutes after bombardment.

IV. CASCADE-EVAPORATION CALCULATION

To compare the results of this investigation with the predictions of the cascade-evaporation model, we decided to use the results of the published Monte Carlo calculations. Since our experimental results are a measure of the final products, it is necessary to use the sum of the cascade and evaporation steps. As mentioned earlier (Sec. I-B), the results of the Metropolis et al. calculation are the best available indications of the cascade step.[24,25] Although the evaporation process has also been studied by the Monte Carlo technique, there are no calculated results available with which our experiments could be compared. However, Alexander, Altman, and Howry[73] have re-programmed the Dostrovsky, Fraenkel, and Friedlander[35] calculation (which will be referred to as the DFF calculation) for use with the IBM 7090 computer. They have made their program, called NEM I, available for our use. After suitable changes, discussed below, the program fulfilled our requirements. However, before progressing to the NEM calculations, it is instructive to review the initial calculations upon which ours is based.

A. Metropolis Cascade Calculation

The nucleus was represented by a degenerate Fermi gas of nucleons in a square-well potential of radius 1.3×10^{-13} cm $A^{1/3}$. The Fermi gas was assumed to remain in its lowest state throughout the cascade process. Tables of the nuclear characteristics for the target nuclei were read into the computer. For the case of ruthenium, the Fermi energies, $E_{F,p} = 26.2$ MeV and $E_{F,n} = 30.7$ MeV were used with an average binding energy of 7.9 MeV for the most loosely bound nucleon to give total nuclear potentials of $V_p = 34.1$ MeV and $V_n = 38.6$ MeV. The Coulomb energy at the surface of the nucleus was taken as 10.5 MeV. In addition, a "cutoff" energy of 46.8 MeV designated the point of termination for the cascade of both neutrons and protons. This value was obtained from an estimation of the kinetic energy that a proton would need to overcome the Coulomb barrier.

The elementary cross sections were the total p-p and n-p scattering cross sections taken as a function of energy and angle. The Coulomb contribution was neglected and the n-n cross sections were assumed to be the same as the p-p. At the lower energies, the experimental values were fitted by

$$\sigma_{ii} = \left(\frac{10.63}{\beta^2} - \frac{29.92}{\beta} + 42.9\right) \text{mb}, \qquad \text{(IV-1)}$$

and

$$\sigma_{ij} = \left(\frac{34.10}{\beta^2} - \frac{82.2}{\beta} + 82.2\right) \text{mb}, \qquad \text{(IV-2)}$$

where β is the velocity of the incident particle in terms of the velocity of light, σ_{ii} refers to collisions between like particles, and σ_{ij} refers to collisions between different particles. For the higher energies, a table of cross sections was read into the computer, and linear interpolation between the values was performed. The angular dependence of the scattering process was given by:

$$d\sigma/d\Omega = K(A \cos^4\theta + B \cos^3\theta + 1), \qquad \text{(IV-3)}$$

where the constants were dependent upon the type of collison.

For the energy region where meson production was believed to become important, both single- and double-pion production, pion scattering and charge exchange, and absorption were included. This information was, in general, tabulated and read into the computer with the use of linear interpolation for intermediate values. A fraction of the nucleon-collision was calculated to lead to pion production which was subdivided into single- and double-pion production which in turn was further subdivided into π^0, π^- and π^+ production. The angular distribution for the pion scattering was given by Eq. (IV-3) with the values of A and B obtained by a least-squares fit to the experimental data. Meson absorption was assumed to

take place by a two-nucleon mechanism and was estimated from the cross sections for deuterons. The experimental data for all this information was fragmentary, and the pion contributions were therefore included with large uncertainties.

Relativistic kinematics and three-dimensional geometry were applied throughout the calculation, and the identity of all particles was maintained. The calculation proceeded by the general Monte Carlo technique (see Sec. I-B). The cascade was followed until all the cascade particles had reached the cutoff energy or had escaped. The excitation energy of the residual nucleus was then the sum of the energy associated with the "holes" in the Fermi gas and the energy of the excited nucleons which were "bound" by the cutoff energy. The information of the cascade was tabulated according to:

(1) The type, energy, and angle of escape of all particles.

(2) The number, type, and energy of the nucleons struck in the cascade.

(3) The atomic number, mass, excitation energy, and momentum of the residual nuclei.

About 1000 cascade cases were computed for each of a number of targets and bombarding energies for protons, neutrons, and pions.

Our interest is primarily that of representing the cascade process for niobium. However, niobium was not one of the target materials for which the cascade process was calculated. Therefore the results for the hypothetical ruthenium-100 were converted to niobium. The conversion consisted of subtracting 3 units from the atomic number and 7 units from the mass of the residual nuclei formed in the cascade process for ruthenium-100. This procedure for converting the cascade results has been utilized before with the assumption that the errors are within the accuracy of the calculation.[37,38] The actual information taken from the cascade calculation was the atomic number, mass and excitation energy of the residual nuclei produced from the theoretical bombardments of protons on ruthenium-100 at 462, 944, and 1844 MeV. The mechanics

of the operation involved taking the information from magnetic tape and punching it on IBM cards which then could be used for the input of the NEM I calculation. This was done by a computer program.

B. The DFF Evaporation Calculation

The initial motivation behind the DFF calculation was to determine how well the statistical theory could explain low-energy (< 50 MeV) reactions. Due to the low excitation energies involved, the authors were required to modify the earlier Dostrovsky, Rabinowitz, and Bivins calculation which was primarily designed to study high excitation-energy events.[33] Although both of these calculations were originally designed to study the systematics of the evaporation process, their success, some of which will be mentioned below, has led us to use the latter to represent the de-excitation process of the cascade-evaporation model. The DFF calculation rather than the initial Dostrovsky et al. calculation is required for this task, because the spectrum of excitation energies produced in the cascade process include the low deposition-energy processes for which the initial calculation is ill suited.

The DFF calculation used Weiskopf's formulation for the probability per unit time of emitting a particle j with kinetic energy between ϵ and $\epsilon + d\epsilon$ as the basis for a computer program. The expression is

$$P_j(\epsilon)d\epsilon = \left[\frac{g_j m_j}{\pi^2 \hbar^3}\right] \sigma\epsilon(W_f/W_i)d\epsilon \qquad \text{(IV-4)}$$

where W_f and W_i are the level densities of the final and initial nuclei at their respective excitation energies, σ is the inverse cross section, m is the mass of the emitted particle, and g is the number of spin states the particle has. The inverse cross sections, level densities, and limits of integration require special attention.

The neutron inverse cross section was approximated from continuum theory to include the energy and mass dependence. The emprical

expression used was

$$\sigma_c/\sigma_g = \alpha\,(1 + \beta/\epsilon), \qquad \text{(IV-5)}$$

where σ_c and σ_g are the capture and geometric cross sections ($\sigma_g = \pi R^2$); the constants were obtained by fitting to continuum theory. Although Eq. (IV-4) applies to the cross sections of a nucleus in an excited state, the ground-state cross sections were used as an approximation. For the case of charged-particle emission, the Coulomb barrier must be taken into account. An empirical equation of the form

$$\sigma_c/\sigma_g = (1 + c_j)\,(1 - k_j F_j/\epsilon)\,, \qquad \text{(IV-6)}$$

was employed. The factor $(1 - k_j V_j/\epsilon)$ expressed an approximation of the quantum mechanical effects of the barrier, and again continuum theory was used to obtain the constants. The barrier was calculated from the classical expression

$$V_j = zZ/r_0 A^{1/3} + \rho_j, \qquad \text{(IV-7)}$$

where z and Z are the atomic numbers of the emitted particle and residual nucleus, e is the electron charge, and ρ_j is an approximation for the radius of the emitted particle. Good agreement was obtained with predictions of continuum theory for all of these expressions.

The level-density expression chosen for this calculation was

$$W(E) = C \exp\{\,2\,[a(E - \delta)^{1/2}]\}\,, \qquad \text{(IV-8)}$$

with $a \propto A$ and with the δ value introduced to take into account the odd-even pairing energy effects by displacement of the ground-state energies forming a "characteristic" level. For a more complete rep-

resentation, the shell effects could also be included in the same way. The DFF authors added this refinement but left the δ value as a parameter to be fitted from a comparison with experimental data.

If the maximum energy available for the evaporation process is

$$(\epsilon_n)_{max} = E - Q_n - \delta_n \quad \text{for neutrons and} \quad \text{(IV-9)},$$

and $$(\epsilon_j)_{max} = E - Q_j - k_j V_j - \delta_j \quad \text{for charged particles} \quad \text{(IV-10)},$$

then the integration is carried out over the range of 0 to $E - Q_n - \delta_n$ for neutrons and $k_j V_j$ to $E - Q_j - \delta_j$ for charged particles. The Q_n and Q_j are the separation energies for neutrons and charged particles. However, these expressions are not entirely valid because of the possibility of energy levels below the characteristic level. The error introduced by this approximation is believed to be small except for the emission of neutrons where the possibility of evaporating to the ground state is quite large. In fact, it has been shown to shift the thresholds upward for specific cases and thereby distort the calculated excitation functions.

A combination of Eqs. (IV-4) through (IV-10) upon integration and with the assumption that

$$\exp[2(a_n R_n)^{1/2}] \gg 1 \quad \text{(IV-11)}$$

yields the neutron-emission probability

$$\Gamma n \approx [(m_n r_0^2)/(2\pi\hbar^2)] \exp\{-2[a_0(E - \delta_0)]^{1/2}\} A_n^{2/3} [g_n \alpha / a_n^2] \exp[2(a_n R_n)^{1/2}]$$

$$\times \{2a_n R_n - (3/2 - a_n\beta)[2(a_n R_n)^{1/2} - 1]\}, \quad \text{(IV-12)}$$

where $R_n = E - Q_n - \delta_n$. (IV-13)

With the assumption that

$$\exp\left[2(a_j R_j)^{1/2}\right] >> 1 , \qquad \text{(IV-14)}$$

one obtains for the probability of charged-particle emission

$$\Gamma_j \tilde{=} [(m_j r_0^2)/(2\pi\hbar^2)] \exp\{-2[a_0(E - \delta_0)]^{1/2}\} A_j^{2/3}[g_j(1 + c_j)/a_j^2]$$

$$\times \exp\left[2(a_j R_j)^{1/2}\right] \{2a_j R_j - (3/2)[2(a_j R_j)^{1/2} - 1]\} \qquad \text{(IV-15)}$$

where $$R_j = E - Q_j - k_j V_j - \delta_j . \qquad \text{(IV-16)}$$

These equations were used to calculate the relative probabilities for the emission of neutrons, protons, deuterons, tritons, helium-3 ions, and helium-4 ions.

The kinetic energy of the emitted particles was selected from a distribution calculated from the original Weisskopf formalism. It was expressed by

$$P(X) = (X/X_{max}) \exp\{a_j X_{max} - [a_j(R_j - X)]^{1/2}\} , \qquad \text{(IV-17)}$$

where $X = \epsilon - V$ with $V = k_j V_j$ for charged particles, $V = -\beta$ for neutrons, and X_{max} is given by

$$X_{max} = (1/a_j)[(a_j R_j + 1/4)^{1/4} - 1/2]. \qquad \text{(IV-18)}$$

However, to conserve computer time, the high-energy tail was approximated by a Maxwellian distribution,

$$P_M(X) = (X/X_{max}) \exp[1 - (X/X_{max})]. \qquad \text{(IV-19)}$$

A list of all the constants required by the calculation were read into the computer and linear interpolation was performed to obtain the intermediate values. Whenever possible, the experimental Q values were employed. If experimental values were not available, the computer calculated them from Cameron's semi-empirical mass formula.[74] The input information consisted of atomic number, mass excitation energy, and number of evaporation chains to be followed for each starting nucleus. In addition, the parameters r_0 and "a" could be changed. A random number selected the particles to be emitted from the relative emission probabilities for each of the particles. These probabilities were calculated by the computer at each step of the chain. Other random numbers suitably selected the kinetic energy of the particle from the kinetic-energy distributions calculated by the computer. This information determined the product, and the procedure was repeated until the R values [Eqs. (IV-13)(IV-16)] for all particles were ≤ 0. The calculation then proceeded to the next evaporation chain.

The information obtained from this calculation is

(1) Type, number, and energy of emitted particles.

(2) Type, number, and residual excitation energy of the final products.

(3) Detailed evaporation paths of each evaporation case.

This is far too much information to be assimilated, and therefore the computer was used to summarize the results in a manner which was convenient for the individual problem. A summarization procedure will be given in connection with our calculation.

C. Present Calculation.

Our calculation consisted of taking the results for ruthenium-100 from the Metropolis et al. calculation, converting them to represent the cascade process for niobium-93, and using them as the input information for the NEM I calculation. The NEM I performed the evaporation calculation giving the results of the cascade-evaporation model. Our

requirements necessitated a summary of the information which would allow a comparison with experimentally determined cross sections. A computer program, NEM IV, was therefore written to give:

(1) A detailed print-out of the evaporation chain.

(2) A summary of the type and number of emitted particles.

(3) A summary of the final products which listed, in order, the Z, A, number, and fraction of the total number of products.

With this information it was possible to compare the calculation with experimental cross sections.

For the calculated results to be physically meaningful, some attention must be given to the input information and parameters used. We have no control over those for the cascade calculation and although there are indications that some of the input information could be improved (i.e., nuclear boundary, meson production, etc.), we are obliged to accept the results as the best available. A new cascade calculation is presently being programmed at Brookhaven National Laboratory in which some of these uncertainties are being corrected. It will be interesting to see if the new calculation is able to rectify the disagreements with experiment. However, we can investigate those parameters which are connected with the evaporation calculation. They are the δ values, r_0, the level densities, and the number of emitted particles.

The DFF authors obtained good agreement with experimental data for a set of δ values which included both pairing energies and shell effects. Their δ values were determined by fitting to experimental data with a choice of $r_0 = 1.5 \times 10^{-13}$ cm. Although the agreement with experimental data is good, the δ values have no physical meaning and are therefore not as satisfactory as could be hoped. Cameron has listed a set of pairing—energy δ values which are a result of his semiempirical mass formula.[74] Upon the observation of the DFF authors that good agreement could be obtained with the use of the Cameron values and a

larger r_0 value, it was decided to use the Cameron δ values. The larger r_0 value arises from the work of Scott[75] and Evans[76] who showed that a nuclear square-well potential with $r_0 = 1.65 \times 10^{-13}$ cm would approximate the smaller diffuse-edge potential obtained in electron-scattering experiments. Our calculation was therefore performed with Cameron pairing-energy δvalues and $r_0 = 1.7 \times 10^{-13}$ cm. Subsequently, Wilkins[77] has shown that for the case of low excitation energy (< 50 MeV), still better agreement is possible if Cameron's shell effects are also included, especially in the region of Z = 28. Altman[78] using higher excitation energies (> 70 MeV) and observing the evaporation products, has not seen a difference between the two sets of Cameron δ values. Since our case represents the latter, only with even greater excitation energies, it was not deemed feasible to repeat our calculations with the values corrected for shell effects, for it would have taken more computer time than was warranted. However, it is possible that some effect might be noticed for the products of Z = 28 and immediately below.

The choice of the level-density parameter "a" has generally been dictated by agreement with experimental data. Thus the DFF authors have stated the perference for a = A/20 when dealing with low excitation energies whereas Dostrovsky et al.[37] have stated that a = A/10 is a better representation of the high excitation-energy processes. A still further complication is the dependence of the best value for "a" upon the r_0 value used. Dostrovsky et al. have shown that a change in the interaction radius is comparable to a change in "a".[37] Although these observations are not completely studied, they serve both to illustrate the confusion concerning the level densities and to question the expression itself (see Igo and Wegner[79]). One feature common to these observations of the level density is the fact that they are based upon the results of the emitted particles. Another approach might be in the investigation of the distribution of the final products. More will be said concerning this point below. With this background of uncertainty

about the "a" parameter, it was decided to carry out the calculation with both a = A/20 and A/10.

The DFF calculation studied the evaporation of six particles: neutrons, protons, deuterons, tritons, helium-3 ions, and helium-4 ions. The success of the calculation in reproducing and experimental data led Dostrovsky et al. to increase the number of emitted particles to fifteen.[37] The calculation was able to predict the results for the isotopes of lithium and beryllium. However, when Dostrovsky, Fraenkel, and Hudis tried to extend the calculation to explain the production of nitrogen-13, the agreement was not satisfactory.[38] Our main interest is in obtaining the distribution of final products rather than studying the emission of small particles. The effect of including the larger number of emitted particles should not cause a great change in the distribution of final products due to their relatively low cross sections. However, we decided to check this parameter by allowing all sixteen particles to evaporate for one calculation. The situation where they would have the greatest effect would be at the highest excitation energies. Therefore, the cascade results for the theoretical bombarding energy of 1844 MeV were chosen and the value of a = A/20 was selected. We found that with the radius given by

$$R = [1.7(A_1^{1/3} + A_2^{1/3}) - 1.2] \times 10^{-13} \text{ cm} \quad \text{(IV-20)}$$

for the heavier particles (>He), where A_1 and A_2 refer to the product nucleus and emitted particle, the heavier particles constituted only 4% of the total emitted particles (see Table A-IV). In addition, they were predominantly emitted in those cases where excitation energies of > 500 MeV were involved, The effect was a slight increase of the lower portion of the mass yield curve (see Fig. 17). Since the effect is small, we decided to represent the evaporation process with the emission of only the six particles used by DFF.

One dominant feature which became evident in the study of the products from the high-energy bombardments is the difficulty in obtaining statistical accuracy with reasonable expenditures of computer time. With the increase in bombarding energy, the number of evaporated particles and the number of final products increases. All of these conditions cause a decrease in statistical accuracy per unit time expended for the calculation. This situation is balanced against computer time with the result that the statistical accuracy becomes poorer as the bombarding energy increases.

The Metropolis et al. calculation represented the cascade process for ruthenium-100 by 809 cases at 462 MeV, 695 cases at 944 MeV, and 402 cases at 1844 MeV. Assuming a total cross section of $\approx$ 1200 mb, the limits of detection for the calculation can then be estimated to be $\approx$ 1 to 2 mb at 462 and 944 MeV, and $\approx$ 3 mb at 1844 MeV. We have calculated five evaporation chains for each initial cascade case. This addition increases the statistical accuracy of the results but should not be taken as improving the limits of detection by a full factor of 5. Since we are interested in increasing the limits of detection of the calculation as far as possible, the results were treated in the following manner in an effort to arrange the data in a form in which a systematic extrapolation could be accomplished. The treatment also makes it possible to study the effect of the parameters in a convenient manner.

The isobaric distribution of the product nuclei was assumed to be Gaussian. The probability Px that x is between x and x + dx is then

$$dPx = (1/\sqrt{\pi}\sigma)\ \exp\ [-(x - m)^2/2\sigma^2]dx, \qquad \text{(IV-21)}$$

where m is the most probable value, x is the measured value, and σ is the standard deviation which describes the width of the distribution.[80] If the fraction of the total, $\sum_1^i x_j/\sum_1^T x_T$, is plotted versus a probability

scale, Px, then a Gaussian distribution forms a straight line with the most probable value[81] determined by Px = 0.500. In addition σ can be found from the fact that for Px = 0.880, the value for $m + \sqrt{2\ell n 2}\,\sigma$ is given. The results of the calculation were fitted to Eq. (IV-21) by this method in which the fraction of the total isobaric yield was plotted as a function of Z + 1/2. It was found that the 1/2 unit of Z was required to account for the drastic step-like behavior of the results. Examples of this treatment are given in Figs. 13 and 14. When an attempt was made to fit the isotopic yield to a Gaussian distribution, it was found that the results formed a curve instead of a straight line.

Initially, the isobaric yleids were plotted as functions of their masses. However, due to the poor statistical accuracy of the calculations, we decided to smooth out the mass-yield curve by an averaging process. Each isobaric yield was represented by the average of three mass units. These averaged mass-yield curves are given in Figs. 15 through 17. Since the most probable Z, Z_p, is determined from the value of Px = 0.500, where the plots of the Gaussian distribution are most accurate, the Z_p values showed relatively little scatter and were therefore plotted without averaging. They are given in Figs. 18 and 19. However, the determination of the σ values involves the slope of the Gaussian plots which are far more susceptible to statistical fluctuations and exhibit considerable oscillation. They were therefore averaged over five values. A plot of these averaged σ values are given in Fig. 20. Standard errors were calculated for a representative selection of the averaged results and found to be less than the graphical fluctuations. The actual numerical values from which these plots were constructed are given in Appendix A.

There are two main features of the results from the calculations. First, the most probable Z values for a given mass seem to be independent of bombarding energy but slightly dependent upon the level-density parameter. Second, σ values, which determine the width of the Gaussian

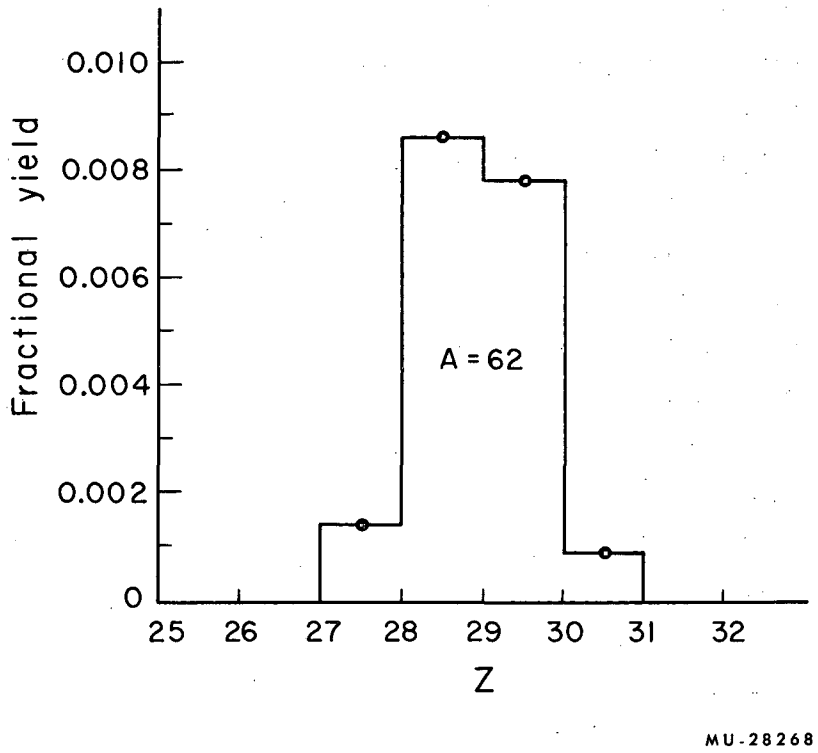

Fig. 13. Distribution of the isobaric yield for A = 62 from the NEM calculation. The data is for 944 MeV, r_0 = 1.7×10^{-13} cm, and a = A/20.

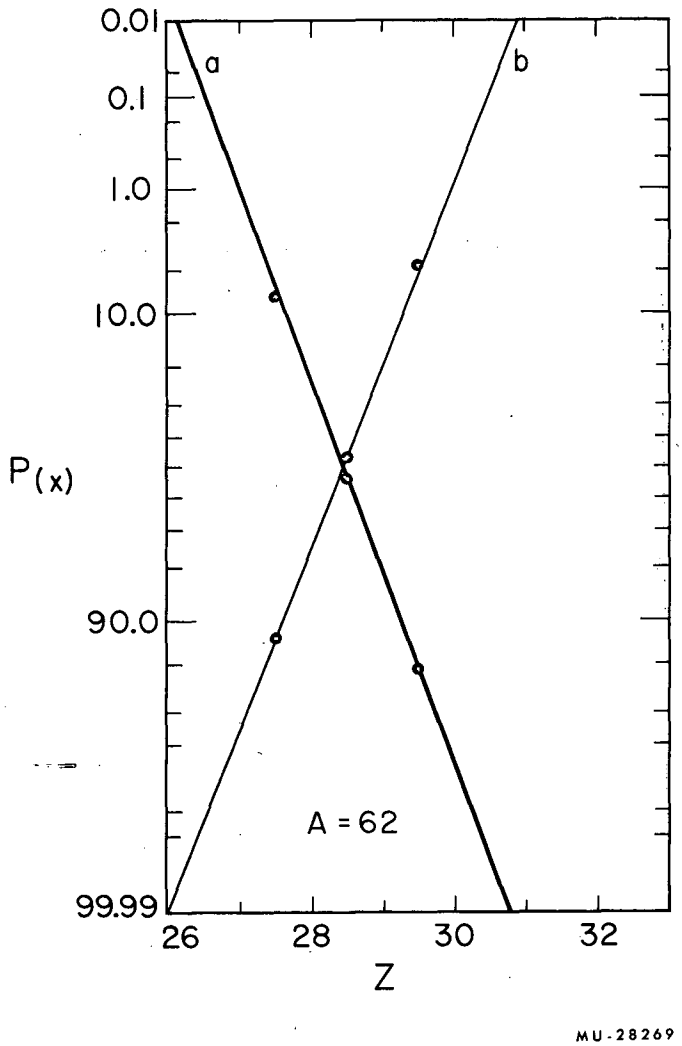

Fig. 14. Probability plot of the data shown in Fig. 13:
(a) Plot initiated from Z = 27.
(b) Plot initiated from Z = 30.

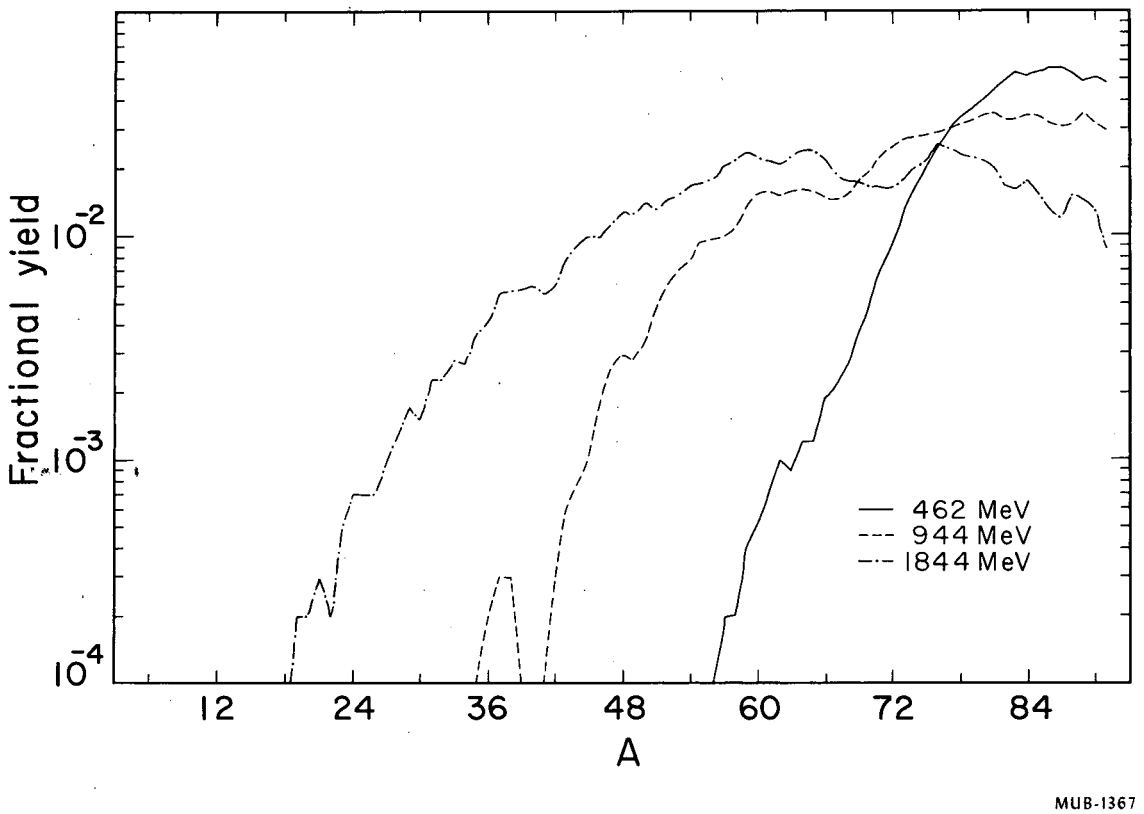

Fig. 15. Averaged mass-yield curve calculated by the NEM calculation. Data is for a = A/10 and the emission of six particles.

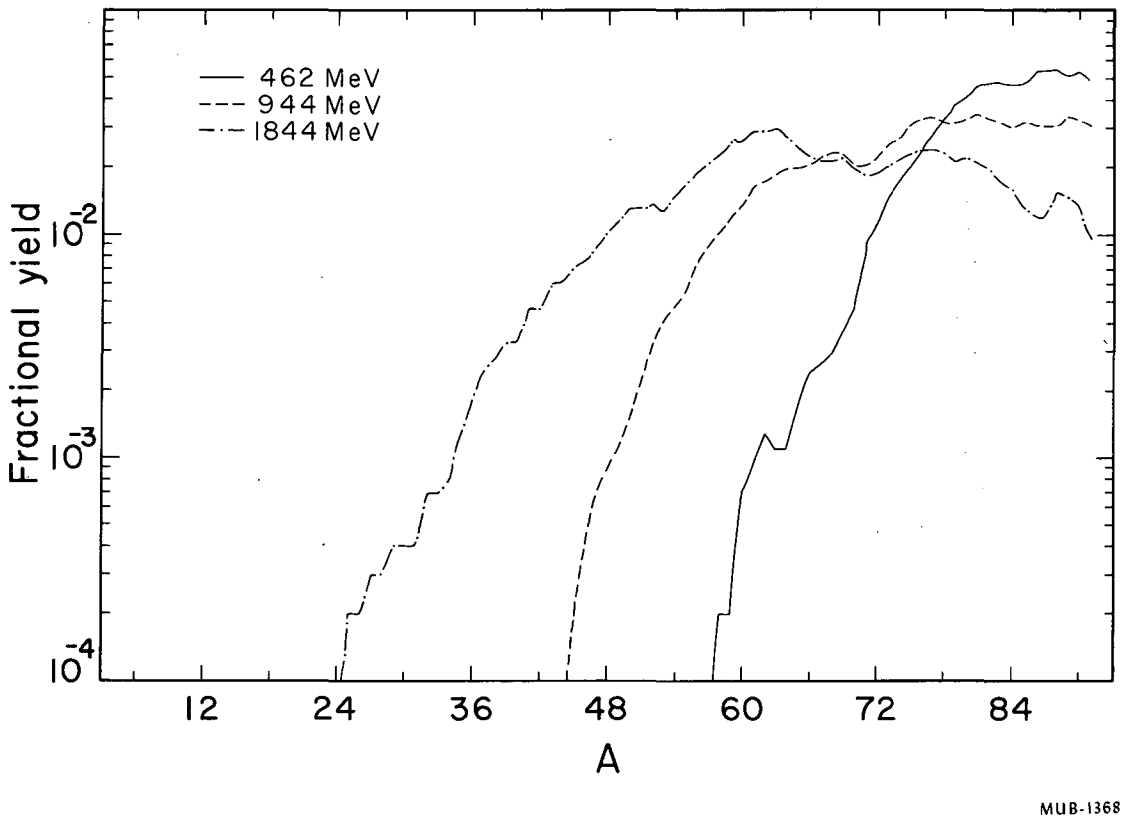

Fig. 16. Averaged mass-yield curve calculated by the NEM calculation. Data is for a = A/20 and the emission of six particles.

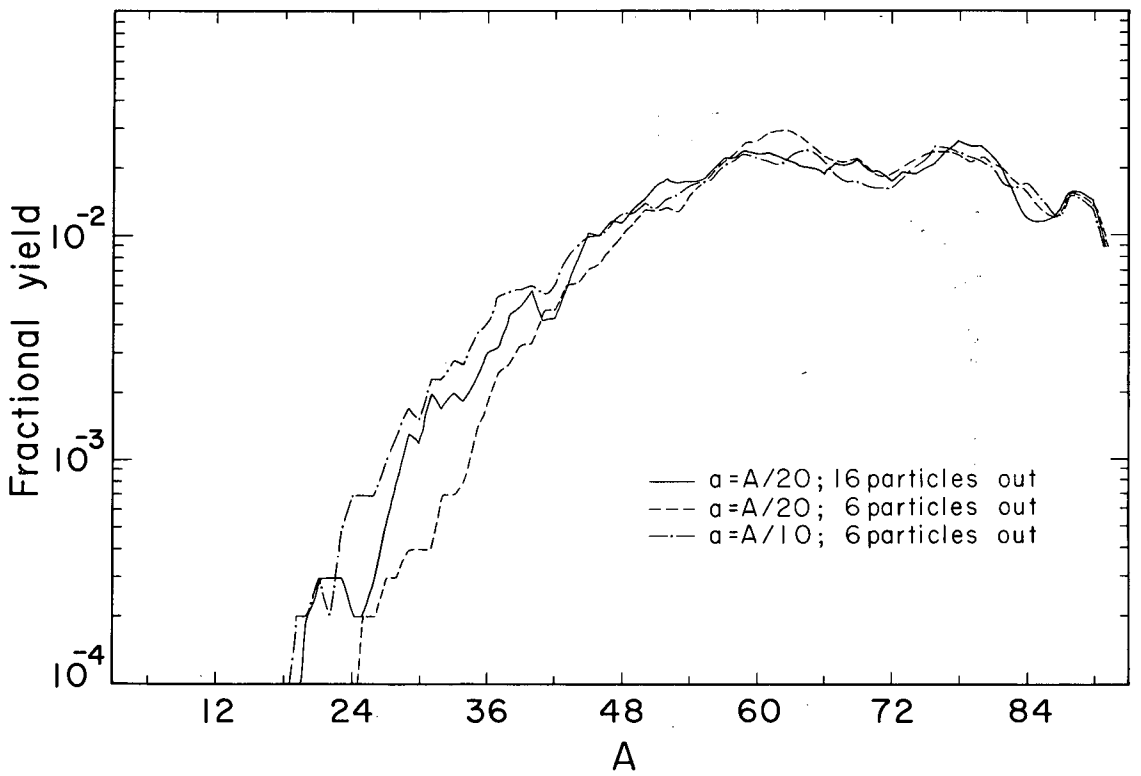

Fig. 17. Averaged mass-yield curve calculated by the NEM calculation. Data is for 1844 MeV incident protons.

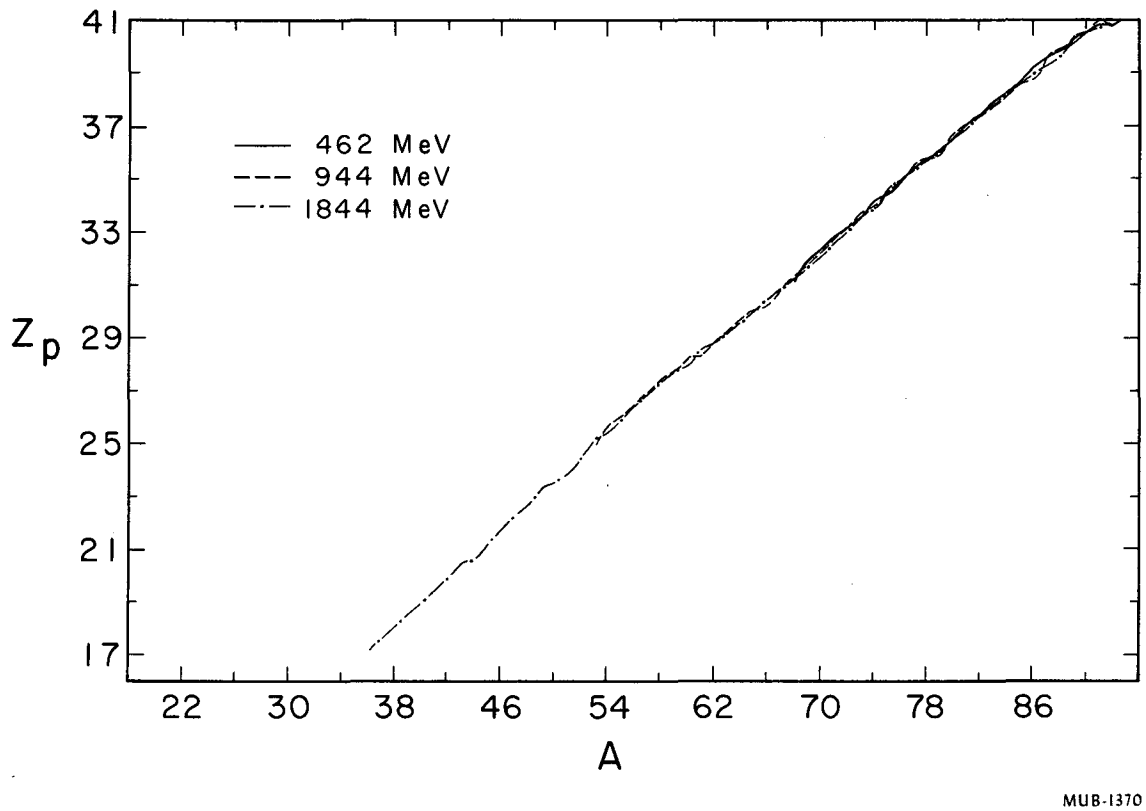

Fig. 18. Distribution of the most probable Z, Z_p, as a function of mass. Data is for a = A/10 and the emission of six particles.

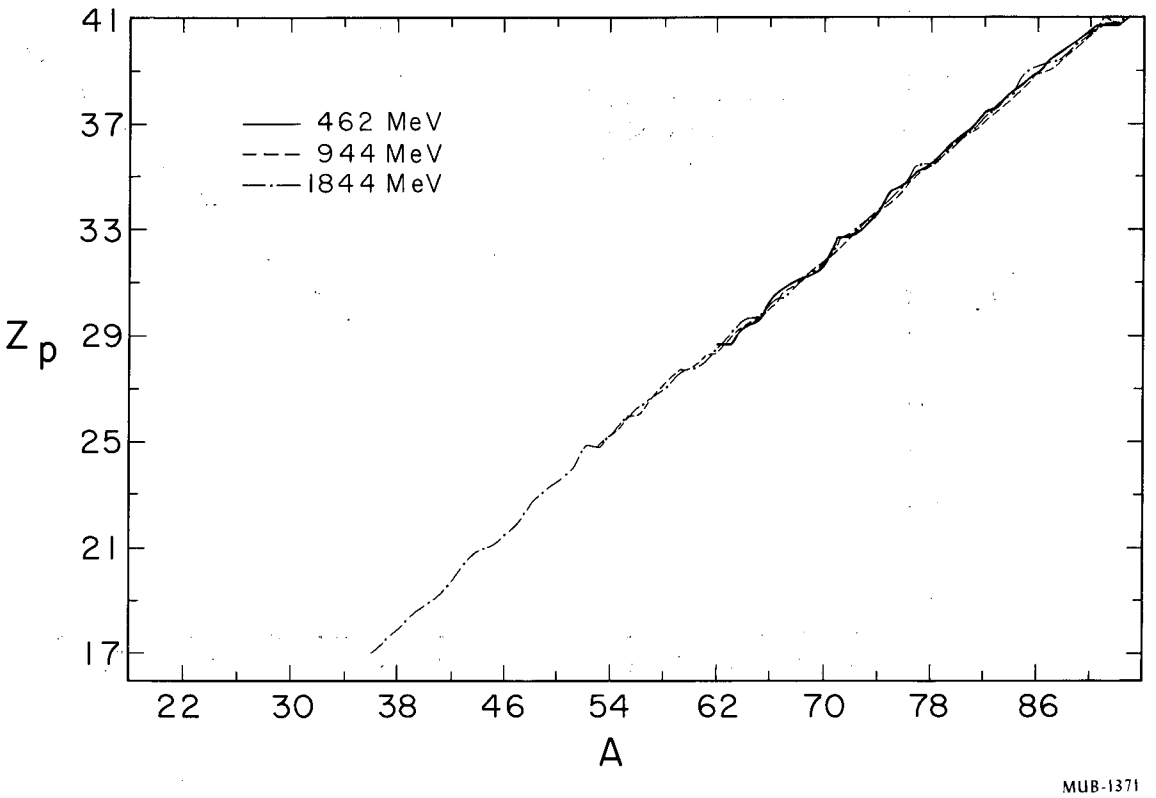

Fig. 19. Distribution of the most probable Z, Z_p, as a function of mass. Data is for a = A/20 and the emission of six particles.

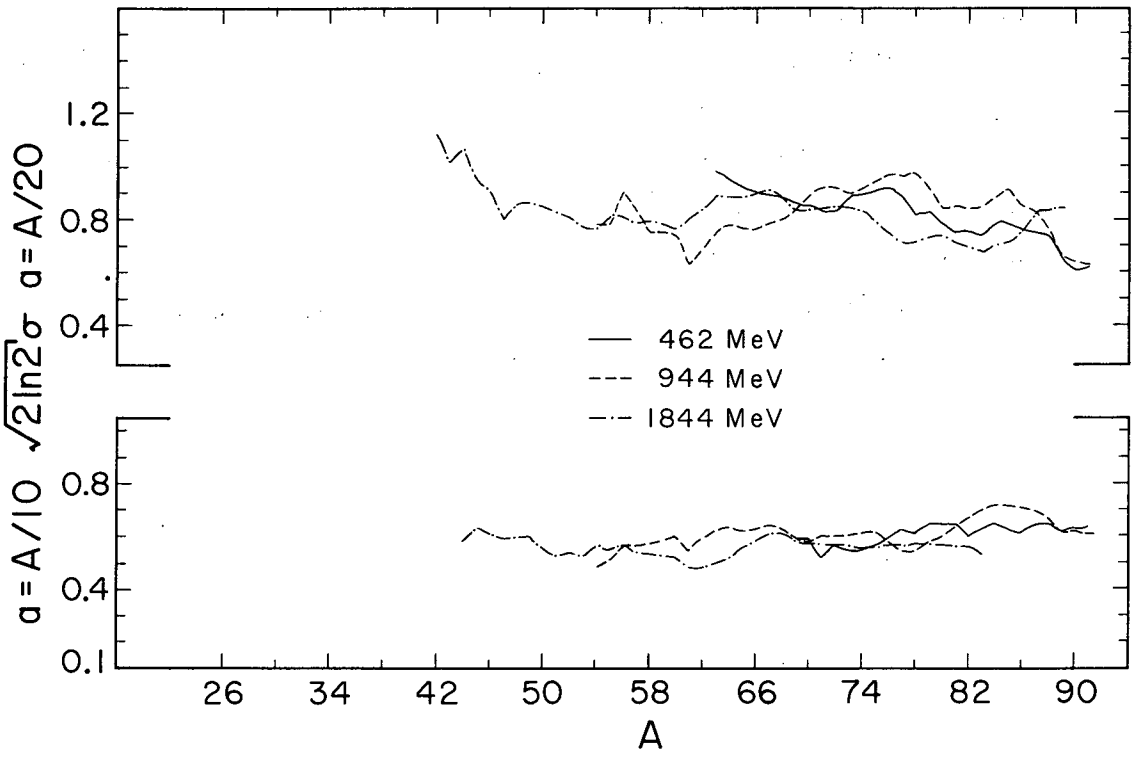

Fig. 20. Distribution of the averaged Gaussian half-widths at half maximum, $\sqrt{2\ell 2}\,\sigma$, calculated by the NEM calculation. Data is for the emission of six particles with a = A/20 and a = A/10.

distribution, are a function of the level density parameter. Since the calculated distributions are such a strong function of σ, a determination of the experimental distribution could determine the best "a" value. For example, Kaufman has determined that isobaric products from the bombardment of arsenic-75 with 2.9 BeV protons yield a Gaussian distribution with the peak displaced by ± 0.35 units of Z from stability and a width at half-maximum of 1.4 charge units.[82] This Gaussian distribution seems to be valid for $66 \leqslant A \leqslant 72$ and would indicate that a $\approx A/15$ would be the best selection for the level-density parameter. It is found (Sec. V-A) that this selection is in agreement with our results.

With the Z_p, σ, and isobaric-yield values, the cross section for any isotope can be calculated once the total cross section for niobium-93 is know. The total cross section was obtained by graphical interpolation of the results of Gooding[83] and was found to be 1230 mb. By using this value for the total cross section, the cross sections for the experimentally determined isotopes of this study were obtained. These values are plotted in Figs. 21 to 24.

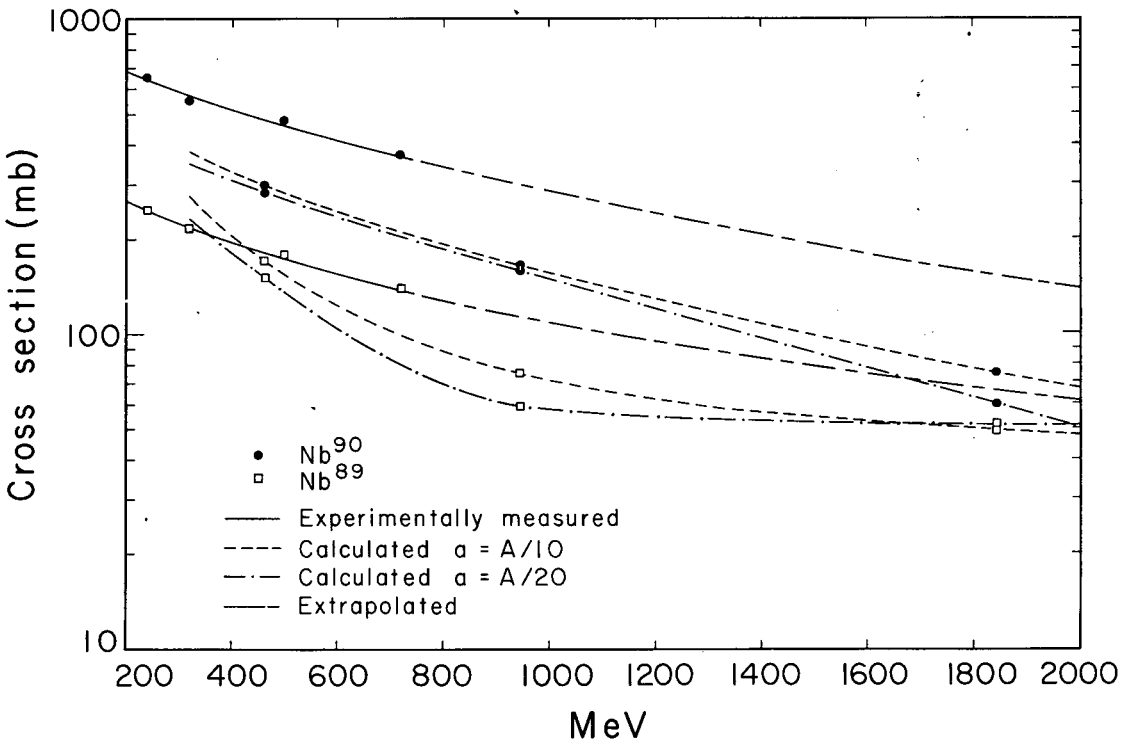

Fig. 21. Excitation functions for the niobium isotopes calculated by the NEM calculation compared with experimentally determined cross sections from proton bombardments. The experimental data is calculated with the sodium-monitor cross section taken as 9.5 mb at 240 MeV and 10.7 mb at 320, 500, and 720 MeV. The total-reaction cross section for niobium was taken as 1230 mb.

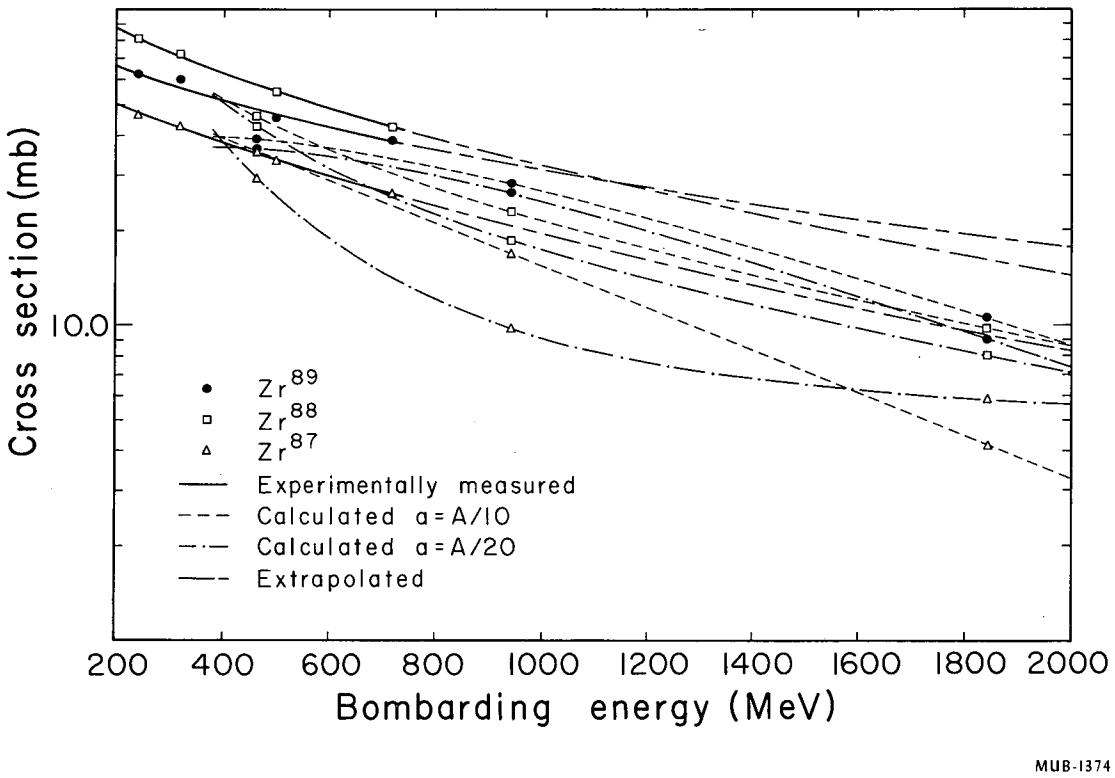

Fig. 22. Excitation functions for the zirconium isotopes calculated by the NEM calculation compared with experimentally determined cross sections from proton bombardments. The experimental data is calculated with the sodium-monitor cross section taken as 9.5 mb at 240 MeV and 10.7 mb at 320, 500 and 720 MeV. The total-reaction cross section for niobium was taken as 1230 mb.

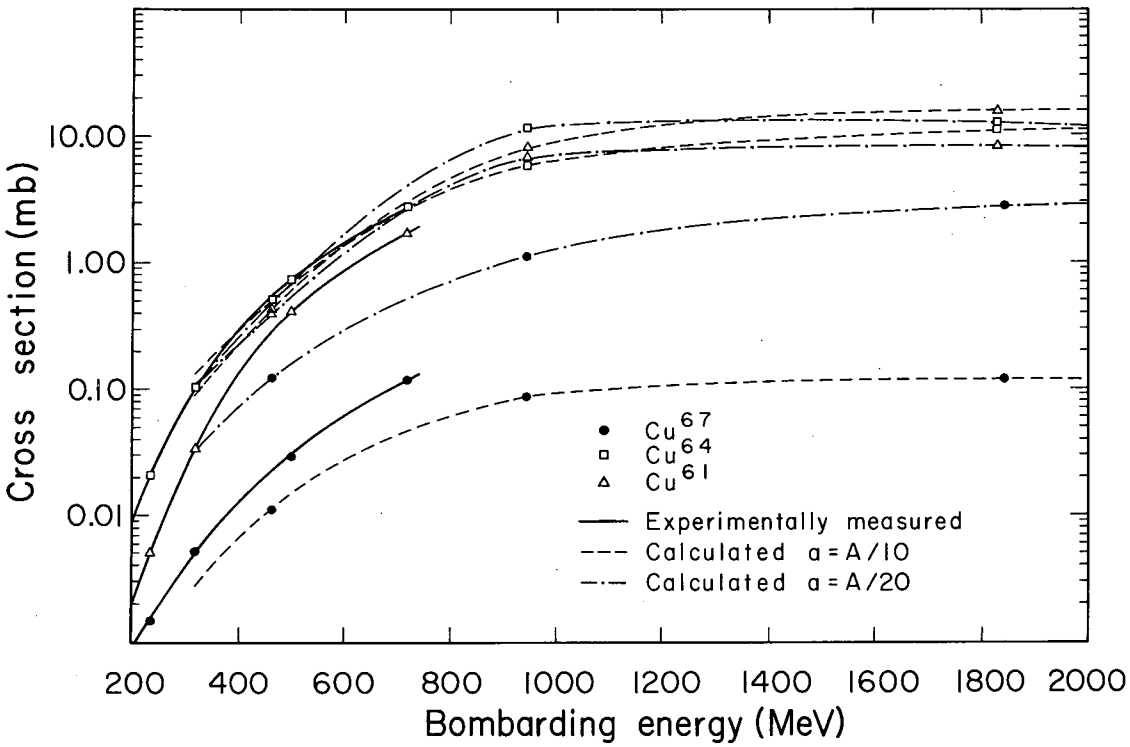

Fig. 23. Excitation functions for the copper isotopes calculated by the NEM calculation compared with experimentally determined cross sections from proton bombardments. The experimental data is calculated with the sodium-monitor cross section taken as 9.5 mb at 240 MeV and 10.7 mb at 320, 500 and 720 MeV. The total-reaction cross section for niobium was taken as 1230 mb.

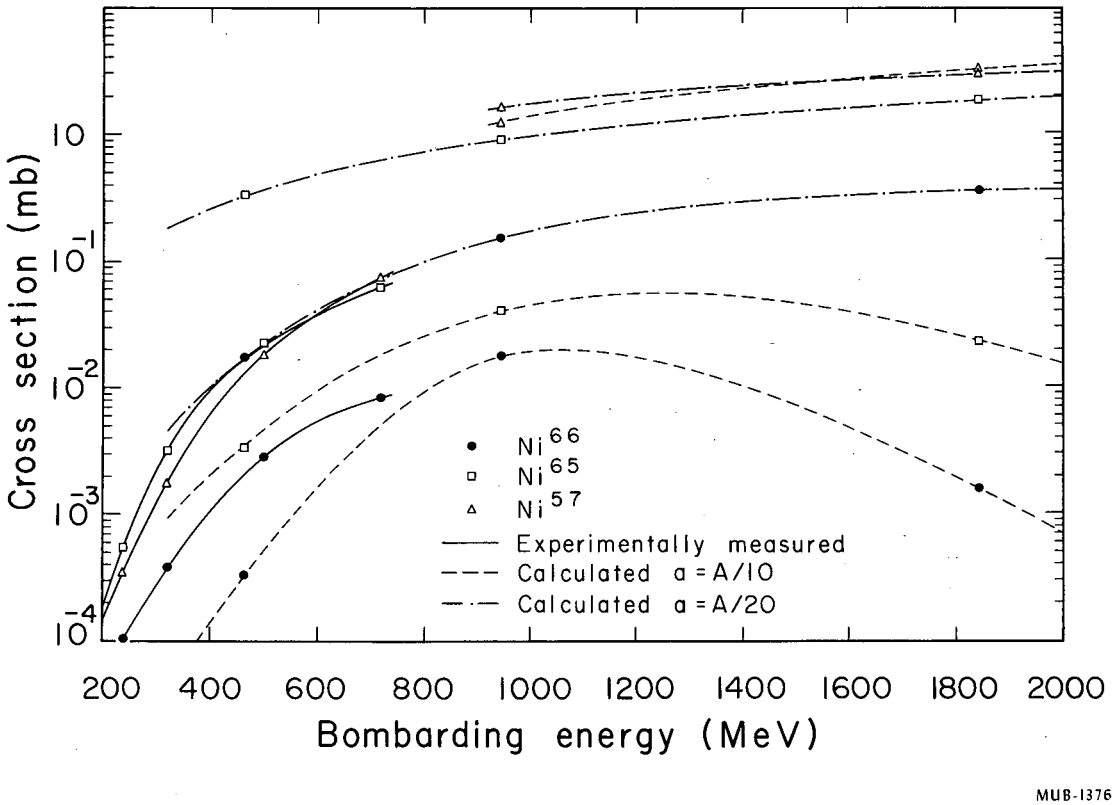

Fig. 24. Excitation functions for the nickel isotopes calculated by the NEM calculation compared with experimentally determined cross sections from proton bombardments. The experimental data is calculated with the sodium monitor cross section taken as 9.5 mb at 240 MeV and 10.7 mb at 320, 500, and 720 MeV. The total reaction cross section for niobium was taken as 1230 mb.

V. DISCUSSION OF RESULTS

A. Comparison of Experimental Results with Those Predicted by the Cascade-Evaporation Model.

Since no one has yet calculated the results of the nucleonic cascade initiated by high-energy helium ions, our discussion in this section is restricted to the results of proton bombardments. It is subdivided according to the deposition-energy required for the formation of the products. Thus the niobium and zirconium results are used to represent the low deposition-energy processes; the copper and nickel results are employed to represent large deposition-energy processes; and the sodium results are used to examine the production of low-mass products. This categorization facilitates the comparison between experimental and calculated results.

1. Low Deposition-Energy Processes.

The niobium and zirconium excitation functions exhibit a gently decreasing slope indicating that their maximum cross sections were obtained at lower bombarding energies than those considered in the present study (see Figs. 3 and 4). Their decrease can be attributed to the competition from processes of higher deposition-energy as the bombarding energy is increased. The decreasing probability for emission of increasing numbers of neutrons in the (p,pxn) reactions is illustrated by the niobium-89 and 90 cross sections. Porile has noted this behavior in a study of the excitation functions for gallium-69 and 71 in which the decrease in cross sections for the (p,pxn) reactions was step-like as the number of emitted neutrons increased.[44] Ladenbauer and Winsberg[84] also noted this behavior in the study of the (p,pxn) reactions of iodine-127.

The behavior of these excitation functions is in general agreement with the predictions of the cascade-evaporation model. The comparison of the experimental and calculated results are plotted in Figs. 21 and 22. If the experimental results are extrapolated to indicate approximate

values for the higher energies, the calculated results show the same qualitative decrease with increasing bombardment energy as the experimental excitation functions. However, the calculation underestimates the measured values for niobium-90 by a factor of $\approx$ 1.7 at 462 MeV, and the factor seems to become greater as the bombarding energy is increased. The agreement is satisfactory for niobium-89 at 462 MeV, but again seems to become poorer at the higher energies. This discrepancy between the predictions of the Monte Carlo calculations and the experimental results for the (p, pxn) reactions has been noted before. Porile found satisfactory agreement for the (p, p4n), (p,p5n), and (p,p6n) reactions at all energies, but noted the underestimation of the (p,p2n) and (p,p3n) reactions at the higher energies.[44] Ladenbauer and Winsburg found satisfactory agreement for the (p,p2n) to (p,p7n) reaction from iodine-127 up to 1 BeV, but noticed an underestimation of the experimental values at 2 BeV.[84] The agreement for the zirconium isotopes is better, although not as good as one could hope. At 462 MeV, the calculation underestimates the values for zirconium-88 and 89 by $\approx$ 25%. The experimental value for zirconium-87 at 462 MeV is bracketed by the calculated values obtained from a change in the level-density parameter of a = A/20 to A/10 . This satisfactory agreement seems to become poorer at the higher energies with a miscalculation of the experimental results by approximately 2 at 1844 MeV. These discrepancies have been taken to indicate an undervaluation of low deposition energy processes by over-rating the importance of meson production in the cascade calculation.

Before undue importance is placed upon the comparison between experimental and calculated results at the higher energies, it must be realized that the extrapolation of experimental results is very uncertain and only presented for an order-of-magnitude comparison. Thus, we can only say that the agreement is satisfactory at 462 MeV for all the measured isotopes of niobium and zirconium except niobium-90, and that this agreement seems to become poorer with increasing bombardment energy.

This finding is in agreement with previous work and indicates that with a suitable adjustment of the parameters and input information (i.e., meson production, level densities, etc.), the cascade-evaporation calculation could represent the low deposition-energy process.

2. Large Deposition-Energy Processes

The experimental cross sections for copper and nickel isotopes show sharply increasing excitation functions having greater slopes for the neutron-deficient isotopes than for the neutron-excess isotopes (see Fig. 5 and 6). These are the qualitative properties that the cascade-evaporation model would predict for the products of large deposition-energy processes. The actual results of the calculation are plotted in Figs. 23 and 24.

Considering the limits of detection and statistical accuracy for the calculation (see Sec. IV-C), its predictions for the production of copper-64 is in excellent agreement with the measured excitation functions. Although the calculation slightly overestimates the values for copper-61, the agreement must be considered satisfactory. The two choices for the level-density parameter "a" liberally bracket the experimental values for copper-67. This large difference in calculated values for copper-67 from the change in "a" is a results of the sensitive dependence on the σ values obtained in the Gaussian fits to the data. Since the copper-67 is removed quite a distance from its Z_p, the effect becomes large (see Sec. IV-C). Therefore, a suitable choice of "a" might be sufficient to obtain agreement for copper-67. A value for "a" closer to A/10 than A/20 would seem to improve the comparison for copper-64 and 61 also. However, the calculation would continue to overestimate the copper-61 cross sections unless some unreasonable value for "a" is used. This fact might indicate that the Z_p distribution is also a cause for the disagreement. If that is the case, more drastic changes in the calculation are required.

The disagreement between calculation and experiment for the nickel isotopes can be attributed in part to two reasons. First, although the results for the copper isotopes are reasonable, the lower cross sections for the nickel isotopes places them almost below the detection of the calculation. Second, nickel-65 and 66 are removed quite a distance from the maximum of their isobaric distributions. The same difficulties in the calculation as were experienced in the case of copper-67 would be expected for these nickel isotopes. Since the experimental results for nickel-65 and 66 lie between the calculated values for a = A/10 and A/20, a suitable choice of "a" could possibly reproduce the experimental values for these two nickel isotopes. However, nickel-57 seems to exhibit the same characteristics as copper-61; that is, no reasonable choice of "a" would bring agreement. Again, it would seem that a change is required which would alter the Z_p distribution.

Although the above disagreements exist between the calculated and experimental values for the copper and nickel isotopes, the general agreement must be considered to be satisfactory when the limits of detection and statistical accuracy for the calculation are assessed. Until the limits are extended for the calculation, we conclude that our results indicate that the calculation, with a suitable choice of parameters, could satisfactorily predict the formation of products of large deposition-energy processes.

3. Production of Low-Mass Products.

The excitation functions for sodium-24 and 22 increase with increasing bombardment energy and are in good agreement with those of Crespo.[45] The greater difficulty in measuring the sodium-22 values is reflected in the scatter of the experimental results for the isotope (see Fig. 7). However, this scatter can not account for the increase in cross section with a decrease in bombardment energy as seen in the proton values at 240 and 320 MeV. This increase is highly unlikely, but since two separate determinations gave the same results, we are obliged to list them.

Upon a closer examination of the excitation functions, two features become evident. First, their slopes are not as great as those for the copper and nickel isotopes. Second, the ratio of neutron-deficient to neutron-excess isotopes decreases with increasing bombardment energy whereas those for the copper and nickel isotopes increase. Both of these features are contrary to the qualitative predictions of the cascade-evaporation model. If the sodium isotopes are produced by the evaporation of particles, their excitation functions should be similar to those of the high deposition-energy processes represented by the copper and nickel isotopes. In fact, both the characteristic steep excitation functions and greater neutron-deficient to neutron-excess ratio with increasing bombardment energy should be more pronounced. Qualitatively, therefore, the sodium results indicate that the cascade-evaporation model does not satisfactorily explain the production of low-mass products.

A quanitative comparison between calculation and experiment substantiates the qualitative predictions. Although the experimental formation cross sections for the sodium isotopes are comparable to those for copper and nickel, the calculation did not predict the formation of any products with mass ≤ 35 until the bombarding energy was raised above 1 BeV. Therefore, the production of the sodium isotopes must have been primarily by a mechanism other than that of the cascade-evaporation model. A number of other authors have also reached this conculsion (see Sec. I-E). Our results can therefore be added to the list of radiochemical studies which require an additional mechanism for the production of low-mass products.

4. Summary

The comparison between our experimental results and those of the Monte Carlo calculations can be summarized in the following manner. In general, the agreement is satisfactory for the low and high deposition-

energy processes. It is felt that with a better set of input information and parameters, good agreement could be expected for a large percentage of the products which are produced by these processes. However, the calculation can not predict the production of low-mass products, and therefore an additional mechanism must be invoked to explain their production.

B. Comparison Between Helium Ion and Proton Results

There is one outstanding feature in the comparison between experimental results from the bombardments of helium-ions and protons. The helium-ion excitation functions parallel those from the proton bombardments for all the isotopes studied (see Fig. 3 through 7). Table VI contains the values for

$$\left(\frac{\sigma_{\alpha,i}}{\sigma_{\alpha,Na}}\right)\Bigg/\left(\frac{\sigma_{p,i}}{\sigma_{p,Na}}\right) = \left(\frac{\sigma_{\alpha,i}}{\sigma_{p,i}}\right)\left(\frac{\sigma_{p,Na}}{\sigma_{\alpha,Na}}\right), \qquad \text{(V-1)}$$

where $\sigma_{\alpha,i}$ and $\sigma_{p,i}$ are the cross sections for isotope i from the bombardment of helium ions and protons respectively, and $\sigma_{\alpha,Na}$ and $\sigma_{p,Na}$ are the corresponding sodium-24 monitor cross sections for aluminum. These ratios have been averaged for each measured energy and show a slight decrease with increasing bombardment energy. The ratios have also been plotted as a function of mass in Fig. 25.

Initially, the experimental cross sections for the production of the isotopes under study were determined relative to the sodium-24 monitor cross section because of the uncertainty in the monitor values. This procedure assumes additional importance because the experimental ratios of these relative cross sections are approximately 1 for a number of different circumstances. Whether the fluctuations in the values, as indicated in Fig. 25 are real can not be determined without further study. However, the persistence of the ratio having a value of ≈ 1 for all of the known cases presents a definite, albeit surprising, comparison between the proton and helium-ion results. This similarity between the helium-ion and proton results is unexpected for two reasons.

Table VI. Ratio of the relative cross sections from helium-ion bombardments to those from proton bombardments.

Isotope	320 MeV	500 MeV	720 MeV	Average
Nb-90	1.04	0.906	0.997	0.981
Nb-89	0.951	0.886	0.886	0.908
Zr-89	0.819	0.801	0.848	0.823
Zr-88	0.894	0.857	0.977	0.909
Zr-87	0.960	0.887	0.947	0.931
Cu-67	0.915	1.08	0.617	0.871
Cu-64	0.737	0.877	0.688	0.767
Cu-61	0.570	0.691	0.663	0.641
Ni-66	1.23	1.13	1.02	1.13
Ni-65	0.852	0.817	0.855	0.841
Ni-57	1.35	0.867	0.865	1.03
Na-24	1.29	1.17	1.02	1.16
Na-22	1.30	1.49	1.19	1.33
Average	0.993±0.066	0.958±0.056	0.890±0.041	

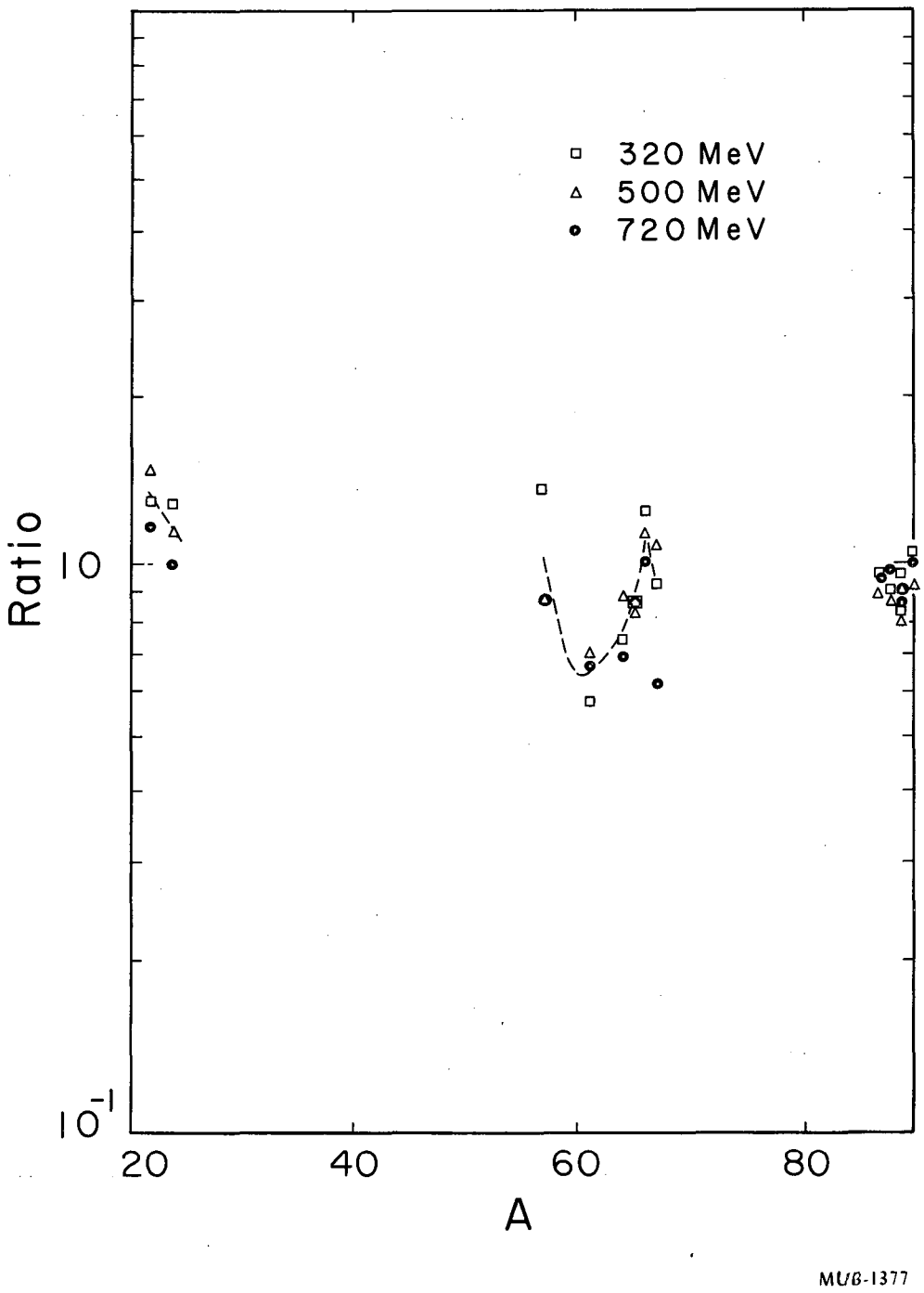

Fig. 25. Plot of the data in Table VI.

First, our study encompasses the energy region in which the production and reabsorption of mesons has been postulated[47] to be the dominant mechanism for the transfer of large amounts of energy to the nucleus. Bethe and de Hoffmann have stated that the most important process for the production of mesons is the collision of two nucleons, whether they are both free particles or one is inside a nucleus.[85] A helium ion as four independent nucleons, each with one-forth the total energy, is then an expedient representation of the helium ion for meson production. Gardner and Lattes were able to show that a 380 MeV helium ion could produce mesons with such a representation.[86] However, they had to use optimum conditions in which both the nucleon within the helium ion and nucleon within the target nucleus were approaching each other at the time of collison. The energy available for meson production would then be

$$E \leq 1/2 \quad (\sqrt{95} + \sqrt{25} + \sqrt{25}) = 195 \text{ MeV}. \qquad (V\text{-}2)$$

Such a depiction of meson production by a helium ion would require that the threshold and subsequent excitation function for the process be displaced from those of a proton of comparable total energy in the energy region of our study. This difference in the ability of the two projectiles to produce mesons should become evident by a variation in the relative probabilities for the formation of products where mesons are believed to play a dominant role. However, the experimental results yield the remarkable similarity between the helium ion and proton.

Second, although at least two different mechanisms are involved, the helium ions are able to reproduce the proton results. From a comparison between the cascade-evaporation calculations and experimental results, we concluded that the sodium isotopes were produced by a mechanism differing from that for the other measured products. The similarity of the helium-ion and proton results is further illustrated in Fig. 26 where

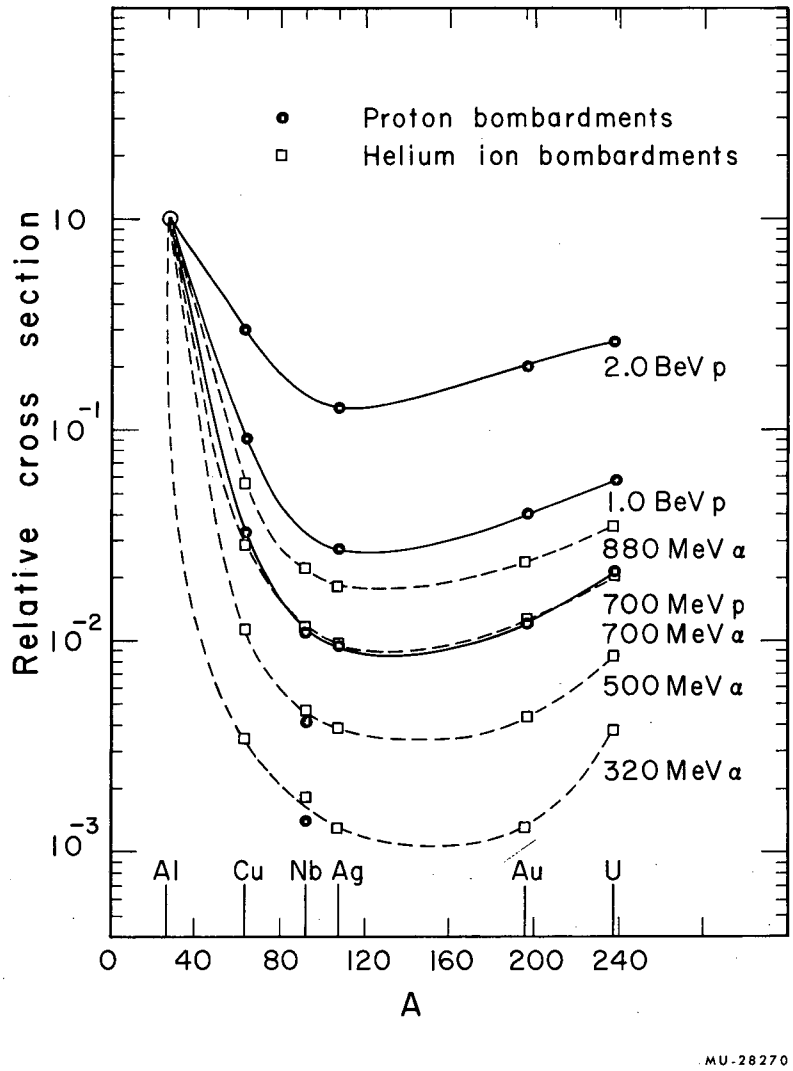

Fig. 26. Formation cross section for sodium 24 as a function of target mass relative to sodium 24 production in aliminum. Data is from references 46, 48, and from the present study.

the relative cross sections for the production of sodium-24 has been plotted as a function of target mass. Again the two projectiles exhibit the same behavior although this representation has been used by Caretto et al.[46] to indicate two different mechanisms for the production of sodium-24. Thus, the helium ion must have high-energy properties such that it is able to undergo the same change in mechanisms as the proton.

The fact that the helium-ion and proton results are similar although their probabilities for meson production are different, would imply that mesons are not a dominant feature of the high-energy reactions. However, before we come to that conculsion, let us consider some of the ramifications.

Sodium, nickel, and copper are the products that we have measured that are believed to be the results of meson production. The Wolfgang et al. fragmentation mechanism for the production of low-mass products, such as sodium, places great importance on mesons.[47] The nickel and copper isotopes are the results of large deposition-energy processes in the cascade-evaporation model. For example, between 270 and 330 MeV of excitation energy was required, on the average, for the production of copper-64 by the evaporation calculation. These high excitation energies are believed to be produced by meson processes in the high-energy cascade.

The implication that mesons are not a dominant feature of the fragmentation mechanism is in agreement with the conculsions at which Crespo[45] arrived from the study of the recoil properties of sodium-24 and magnesium-28. However, we have stated that the cascade-evaporation calculation possibly could predict the production of nickel and copper isotopes. This calculation used the production of mesons to attain the high excitation energies necessary for their production. Thus we are confronted with an inconsistency and must consider two possible explanations for the data.

First, mesons are not a dominant feature of high-energy reactions, and the calculation would be able to predict the same agreement for the

nickel and copper isotopes without the inclusion of meson processes. Second, meson processes are important, and the helium ion is able to produce them with a probability comparable to that of a proton. The measurement of the cross section for meson production in complex nuclei with incident helium ions and a cascade calculation without the inclusion of meson processes would facilitate a decision between these two possibilities. Our results can only point out the inconsistencies.

The fact that the helium ion is able to reproduce the same change in mechanisms which the proton undergoes, indicates that its high-energy behavior is quite similar to that of the proton. A representation of the helium ion as interacting as a unit, at least in the first collision, might be better suited to explain the similarities than a representation of four independent nucleons each with one-forth of the total energy. However, such a representation is in disagreement with the impulse approximation (see Sec. I-A) and complicates the explanation of meson production. Whether either of these two representations of the helium ion is a realistic model can not be determined from the results of this investigation alone. A Monte Carlo calculation with the helium ion represented as four independent nucleons impinging upon the nucleus with a special distribution given by the dimensions of the helium ion would be helpful in determining the relative merits of these two representations. However, it might be found, upon further study, that a quantum mechanical optical model representation is best suited to explain the relative behavior of the proton and helium ion.

The comparison between the experimental results of the proton and helium-ion bombardments can be summarized by the following statements: The helium ion yields results similar to those of the proton in the energy region of our study for a number of different circumstances. Although the true nature of the helium-ion interaction is not known, it seems reasonable that it would have a different probability for meson production than would the proton, particularily in the energy region where the threshold for meson production occurs. This difference in

probability should be evident in the processes where mesons play a dominant role, but we have noticed no such variations. This observation would imply that meson production and interaction are not a dominant feature of high-energy reactions. However, in comparing the proton results with those of the cascade-evaporation model, the calculation showed a possible agreement with the inclusion of meson processes. This inconsistency requires further study for definite resolution. Our results therefore indicate the need for further study of the assumptions inherent in the high-energy reactions.

ACKNOWLEDGMENTS

I am pleased to acknowledge the guidance and interest of Professor Isadore Perlman in this work.

I am especially indebted to Dr. Earl K. Hyde whose encouragement and assistance has been particularly helpful.

I wish to thank Dr. John M. Alexander for many helpful discussions and for the evaporation program and cascade data which he made available. I am grateful to Mr. Lawrence L. Altman for his adaption of the evaporation program to meet the requirements of this study and for his help in its execution. In addition, I am thankful for the program written by Mr. Herbert C. Albrecht for the conversion of the cascade data to a form acceptable by the evaporation program.

The assistance of the 184-inch cyclotron operating crew and the Health Chemistry Group in conducting the bombardments is appreciated. I would also like to thank the Analytical Group for the chemical analysis of many of the samples and Mr. George Shalimoff for the spectroanalysis of target materials.

In addition, I would like to thank Mr. Paul D. Croft and Mr. Bruce D. Wilkins and other fellow students for many discussions, some of which were relevent and helpful.

This work was performed under auspices of the U. S. Atomic Energy Commission.

APPENDIX

A. Results of the NEM Evaporation Calculations

The output of the NEM calculations were treated according to the method described in Sec. IV-C. Tables A-I, A-II, A-III contain these results for the bombarding energies 462, 944, and 1844 MeV respectively. Each table is divided into two sections to accomodate the two values of the level density parameter "a". The first column lists the isobaric yields as a fraction of total yield. The average values for these isobaric yields are given in the second column. The third column contains the Z_p values. The values for $\sqrt{2\ell n2}\sigma$ (half-width at half maximum) and their average values are listed in Columns 4 and 5. Column 6 gives the mass number, and then the table is repeated for the change in the "a" value. These results are for the emission of six particles in the evaporation step: neutrons, protons, deuterons, tritons, helium-3 ions, and helium-4 ions. The fractional yields of the emitted particles are given in Table A-IV.

It is possible to calculate the cross sections for any isotope from these values once the total cross section for niobium is known. The fraction of an isobaric yield which is due to a specific isotope can be obtained by constructing the Gaussian curve for that mass from the values of Z_p and $\sqrt{2\ell n2}\sigma$. To account for the step-like behavior of the results, the isotopic value must be obtained from the value for its Z + 1/2 (see Figs. 13 and 14). For the cases where the data is insufficient, an estimation of the required values can be obtained from Figs. 15 through 20. The cross section for a specific isotope is then

$$\sigma = \sigma_T \, (F_y) \, (F_i) \qquad \text{(A-I)}$$

where σ_T is the total cross section, F_y is the isobaric yield, and F_i is the fraction of the isobaric yield for the specific isotope.

Table A-I. Results of the NEM calculation for 462 MeV incident protons on niobium.

462 MeV; a = A/10; 6 part. out						462 MeV; a = A/20; 6 part. out				
Fract.	Av.	Z_p	$\sqrt{2\ell n 2}\sigma$	Av.	A	Fract.	Av.	Z_p	$\sqrt{2\ell n 2}\ \sigma$	Av.
0.1434		41.00			93	0.1434		41.00		
0.0366		40.74	0.55		92	0.0361		40.71	0.53	
0.0534	0.0483	40.77	0.53	0.635	91	0.0564	0.0496	40.77	0.56	0.615
0.0549	0.0513	40.52	0.71	0.624	90	0.0564	0.0540	40.44	0.69	0.606
0.0455	0.0489	40.20	0.75	0.616	89	0.0491	0.0514	40.12	0.68	0.638
0.0464	0.0528	39.81	0.58	0.650	88	0.0488	0.0545	39.72	0.57	0.738
0.0664	0.0560	39.53	0.51	0.642	87	0.0655	0.0543	39.40	0.69	0.746
0.0551	0.0558	39.09	0.70	0.614	86	0.0487	0.0535	38.88	0.06	0.752
0.0460	0.0529	38.67	0.67	0.624	85	0.0463	0.0467	38.53	0.73	0.780
0.0566	0.0517	38.26	0.61	0.644	84	0.0450	0.0462	38.19	0.71	0.790
0.0524	0.0530	37.87	0.63	0.625	83	0.0474	0.0480	37.58	0.71	0.732
0.0501	0.0585	37.38	0.61	0.598	82	0.0517	0.0472	37.38	0.74	0.748
0.0430	0.0441	37.07	0.62	0.644	81	0.0425	0.0461	36.76	0.77	0.748
0.0393	0.0397	36.55	0.52	0.646	80	0.0442	0.0404	36.38	0.81	0.782
0.0369	0.0366	36.05	0.84	0.646	79	0.0346	0.0383	35.92	0.71	0.826
0.0335	0.0338	35.69	0.64	0.612	78	0.0362	0.0325	35.42	0.88	0.814
0.0309	0.0289	35.49	0.61	0.624	77	0.0268	0.0287	35.18	0.96	0.882
0.0222	0.0247	34.82	0.45	0.590	76	0.0231	0.0235	34.67	0.81	0.914
0.0209	0.0198	34.44	0.58	0.560	75	0.0205	0.0206	34.48	1.15	0.908
0.0163	0.0164	34.22	0.67	0.548	74	0.0182	0.0170	33.71	0.87	0.894
0.0119	0.0127	33.66	0.49	0.540	73	0.0124	0.0148	33.24	0.85	0.890
0.0099	0.0091			0.568	72	0.0138	0.0114	32.74	0.89	0.832
0.0056	0.0072	32.86	0.42	0.515	71	0.0081	0.0092	32.72	0.69	0.828
0.0060	0.0049	32.38	0.69	0.590	70	0.0057	0.0058	31.78	0.86	0.852
0.0032	0.0037	31.92	0.46	0.590	69	0.0037	0.0038	31.31	0.85	0.852
0.0019	0.0026	31.29	0.79		68	0.0021	0.0029	31.14	0.97	0.880
0.0027	0.0021				67	0.0030	0.0027	30.85	0.89	0.892
0.0017	0.0019				66	0.0029	0.0024	30.50	0.83	0.900
0.0014	0.0012				65	0.0012	0.0017	29.30	0.92	0.918
0.0005	0.0012				64	0.0010	0.0011	29.50	0.89	0.952
0.0016	0.0009	29.37	0.88		63	0.0012	0.0011	28.73	1.06	0.983
0.0007	0.0010				62	0.0012	0.0013	28.73	1.06	
0.0007	0.0007				61	0.0015	0.0009			
0.0007	0.0005				60	0.0000	0.0007			
0.0000	0.0004				59	0.0005	0.0002			
0.0004	0.0002				58	0.0000	0.0002			
0.0002	0.0002				57					
0.0000	0.0001				56					

Table A-II. Results of the NEM calculation for 944 MeV incident protons on niobium.

944 MeV; a = A/10; 6 part. out						944 MeV; a = A/20; 6 part. out				
Fract.	Av.	Z_p	$\sqrt{2\ell n2}\ \sigma$	Av.	A	Fract.	Av.	Z_p	$\sqrt{2\ell n2}\ \sigma$	Av.
0.0547		41.00			93	0.0547		41.00		
0.0244		40.75	0.69		92	0.0256		40.77	0.70	
0.0256	0.0297	40.98	0.54	0.615	91	0.0282	0.0306	40.92	0.51	0.630
0.0391	0.0319	40.41	0.56	0.624	90	0.0379	0.0327	40.39	0.59	0.636
0.0311	0.0351	39.99	0.67	0.610	89	0.0311	0.0388	39.91	0.72	0.660
0.0351	0.0315	39.63	0.66	0.670	88	0.0325	0.0303	39.50	0.66	0.762
0.0282	0.0305	39.42	0.62	0.694	87	0.0274	0.0310	39.04	0.82	0.828
0.0282	0.0317	38.69	0.84	0.710	86	0.0331	0.0311	38.83	1.02	0.844
0.0388	0.0344	38.62	0.68	0.712	85	0.0327	0.0319	38.39	0.92	0.908
0.0362	0.0343	38.08	0.75	0.718	84	0.0299	0.0299	37.89	0.80	0.888
0.0280	0.0329	37.72	0.67	0.692	83	0.0270	0.0316	37.50	0.98	0.846
0.0346	0.0331	37.35	0.65	0.672	82	0.0380	0.0329	37.12	0.72	0.842
0.0366	0.0352	37.12	0.71	0.638	81	0.0337	0.0350	36.62	0.81	0.846
0.0343	0.0347	36.60	0.58	0.596	80	0.0334	0.0329	36.33	0.90	0.838
0.0332	0.0326	36.09	0.58	0.574	79	0.0317	0.0318	35.97	0.82	0.908
0.0302	0.0314	35.77	0.46	0.540	78	0.0362	0.0318	35.43	0.94	0.970
0.0308	0.0300	35.59	0.54	0.542	77	0.0334	0.0338	35.16	1.07	0.958
0.0291	0.0292	34.87	0.54	0.572	76	0.0379	0.0329	34.63	1.12	0.970
0.0277	0.0282	34.51	0.59	0.614	75	0.0274	0.0312	34.04	0.84	0.940
0.0279	0.0273	34.01	0.73	0.612	74	0.0284	0.0269	33.69	0.88	0.916
0.0264	0.0272	33.66	0.67	0.602	73	0.0248	0.0253	33.41	0.79	0.892
0.0274	0.0244	33.10	0.53	0.600	72	0.0228	0.0222	32.88	0.95	0.920
0.0193	0.0230	32.80	0.49	0.602	71	0.0191	0.0206	32.33	1.00	0.922
0.0222	0.0192	32.30	0.58	0.576	70	0.0198	0.0206	31.80	0.98	0.896
0.0162	0.0179	31.78	0.74	0.584	69	0.0230	0.0227	31.42	0.89	0.838
0.0153	0.0151	31.23	0.54	0.628	68	0.0253	0.0233	31.03	0.66	0.800
0.0139	0.0145	30.91	0.57	0.638	67	0.0216	0.0219	30.68	0.66	0.786
0.0144	0.0148	30.22	0.71	0.626	66	0.0188	0.0207	30.14	0.81	0.760
0.0162	0.0157	30.03	0.63	0.614	65	0.0216	0.0199	29.72	0.91	0.768
0.0164	0.0162	29.76	0.68	0.636	64	0.0193	0.0198	29.41	0.76	0.782
0.0161	0.0157	29.27	0.48	0.620	63	0.0184	0.0188	29.02	0.70	0.754
0.0146	0.0153	28.84	0.68	0.592	62	0.0187	0.0174	28.42	0.73	0.684
0.0153	0.0159	28.40	0.63	0.546	61	0.0152	0.0165	28.26	0.67	0.626
0.0179	0.0157	28.29	0.49	0.600	60	0.0156	0.0137	27.79	0.56	0.740
0.0138	0.0136	27.71	0.45	0.582	59	0.0104	0.0119	27.71	0.47	0.752
0.0092	0.0109	27.50	0.75	0.570	58	0.0098	0.0103	27.22	1.27	0.750
0.0098	0.0099	26.87	0.59	0.560	57	0.0107	0.0090	26.72	0.79	0.840
0.0107	0.0097	26.53	0.57	0.566	56	0.0066	0.0076	26.03	0.66	0.906
0.0087	0.0094	26.07	0.44	0.504	55	0.0055	0.0056	25.94	1.01	0.782
0.0087	0.0078	25.72	0.48	0.483	54	0.0046	0.0048	25.28	0.80	0.780
0.0061	0.0072	25.00	0.44	0.453	53	0.0044	0.0042	24.85	0.65	
0.0069	0.0060				52	0.0035	0.0033			
0.0049	0.0049				51	0.0020	0.0022			
0.0029	0.0034				50	0.0012	0.0015			
0.0024	0.0028	23.50			49	0.0012	0.0011			
0.0032	0.0030				48	0.0009	0.0009			
0.0035	0.0026	22.08			47	0.0006	0.0007			
0.0012	0.0019				46	0.0006	0.0004			
0.0009	0.0010				45	0.0000	0.0002			
0.0009	0.0008				44	0.0000	0.0000			
0.0006	0.0006				43	0.0000	0.0000			
0.0003	0.0003				42	0.0000	0.0000			
0.0000	0.0001				41	0.0000	0.0001			
0.0000	0.0000				40	0.0003	0.0001			
0.0000	0.0001				39	0.0000	0.0001			
0.0003	0.0003				38					
0.0006	0.0003				37					
0.0000	0.0002				36					
0.0000	0.0001				35					
0.0003	0.0001				34					
0.0000	0.0001									

Table A-III. Results of the NEM calculation for 1844 MeV incident protons on niobium.

1844 MeV; a = A/10; 6 part. out						1844 MeV; a = A/20; 6 part. out				
Fract.	Av.	Z_p	$\sqrt{2\ell n 2}\ \sigma$	Av.	A	Fract.	Av.	Z_p	$\sqrt{2\ell n 2}\ \sigma$	Av.
0.0771		41.00			93	0.0771		41.00		
0.0075					92	0.0075				
0.0100	0.0088				91	0.0105	0.0098			
0.0090	0.0130	40.50			90	0.0115	0.0135	40.35	0.82	
0.0200	0.0145	40.20	0.79		89	0.0185	0.0148	40.08	0.99	0.825
0.0145	0.0155	39.51	0.73		88	0.0145	0.0153	39.40	0.73	0.840
0.0120	0.0120				87	0.0130	0.0122	39.31	0.76	0.826
0.0095	0.0130				86	0.0090	0.0122	39.14	0.90	0.750
0.0175	0.0155	38.64	0.52		85	0.0145	0.0135	38.88	0.75	0.712
0.0195	0.0175				84	0.0169	0.0159	38.06	0.61	0.702
0.0155	0.0162	37.78	0.54		83	0.0164	0.0171	37.70	0.54	0.676
0.0135	0.0168	37.48	0.52	0.558	82	0.0180	0.0198	37.23	0.71	0.692
0.0214	0.0202	36.92	0.52	0.556	81	0.0249	0.0208	36.68	0.78	0.706
0.0285	0.0220	36.66	0.65	0.564	80	0.0195	0.0223	36.32	0.82	0.740
0.0189	0.0224	35.99	0.55	0.574	79	0.0224	0.0213	35.79	0.68	0.732
0.0224	0.0236	35.81	0.58	0.570	78	0.0220	0.0233	35.41	0.71	0.712
0.0294	0.0247	35.63	0.57	0.560	77	0.0254	0.0239	35.47	0.67	0.702
0.0224	0.0254	34.87	0.50	0.566	76	0.0244	0.0239	34.71	0.68	0.744
0.0244	0.0217	34.63	0.60	0.554	75	0.0219	0.0228	34.16	0.77	0.788
0.0184	0.0202	33.89	0.58	0.548	74	0.0220	0.0218	33.78	0.89	0.830
0.0179	0.0180	33.70	0.52	0.564	73	0.0215	0.0203	33.32	0.93	0.840
0.0179	0.0164	33.01	0.54	0.558	72	0.0175	0.0188	32.86	0.88	0.848
0.0135	0.0166	32.65	0.58	0.566	71	0.0175	0.0183	32.66	0.73	0.838
0.0184	0.0166	32.10	0.57	0.568	70	0.0199	0.0199	31.75	0.81	0.840
0.0179	0.0177	31.72	0.62	0.588	69	0.0224	0.0221	31.40	0.84	0.832
0.0169	0.0177	31.39	0.52	0.610	68	0.0239	0.0214	31.04	0.94	0.878
0.0184	0.0189	30.83	0.64	0.604	67	0.0180	0.0215	30.48	0.84	0.906
0.0215	0.0218	30.50	0.69	0.578	66	0.0225	0.0226	30.23	0.96	0.898
0.0254	0.0241	30.02	0.54	0.556	65	0.0274	0.0248	29.71	0.95	0.880
0.0254	0.0244	29.63	0.49	0.516	64	0.0245	0.0279	29.62	0.80	0.884
0.0224	0.0226	29.22	0.42	0.496	63	0.0319	0.0294	29.08	0.85	0.890
0.0119	0.0209	28.87	0.44	0.480	62	0.0313	0.0295	28.58	0.86	0.844
0.0204	0.0217	28.60	0.59	0.476	61	0.0249	0.0289	27.99	0.99	0.802
0.0249	0.0226	27.94	0.46	0.518	60	0.0299	0.0261	27.75	0.72	0.764
0.0224	0.0235	27.81	0.47	0.526	59	0.0234	0.0264	27.58	0.59	0.784
0.0233	0.0219	27.41	0.63	0.532	58	0.0259	0.0229	27.00	0.66	0.796
0.0199	0.0206	26.95	0.48	0.538	57	0.0194	0.0214	26.68	0.96	0.784
0.0185	0.0179	26.57	0.62	0.568	56	0.0190	0.0189	26.30	1.05	0.808
0.0154	0.0173	25.94	0.49	0.546	55	0.0184	0.0171	25.80	0.66	0.816
0.0180	0.0168	25 52	0.62	0.563	54	0.0140	0.0151	25.28	0.71	0.758
0.0169	0.0153	25.13	0.52	0.523	53	0.0130	0.0128	24.78	0.70	0.768
0.0110	0.0148			0.540	52	0.0115	0.0137	24.86	0.67	0.806
0.0164	0.0131	23.87	0.46	0.523	51	0.0165	0.0130	23.95	1.10	0.826
0.0120	0.0141	23.56	0.56	0.550	50	0.0110	0.0132	23.54	0.85	0.844

Continued

Table A-III. (Cont)

1844 MeV; a = A/10 6 part. out						1844 MeV; a = A/20; 6 part. out				
Fract.	Av.	Z_p	$\sqrt{2\ell n 2}\ \sigma$	Av.	A	Fract.	Av.	Z_p	$\sqrt{2\ell n 2}\ \sigma$	Av.
0.0140	0.0127	23.38	0.55	0.600	49	0.0120	0.0115	23.19	0.81	0.862
0.0120	0.0127	22.69	0.63	0.596	48	0.0115	0.0105	22.71	0.79	0.860
0.0120	0.0115	22.29	0.80	0.592	47	0.0080	0.0088	21.92	0.76	0.806
0.0105	0.0100	21.86	0.44	0.613	46	0.0070	0.0075	21.50	1.09	0.904
0.0075	0.0100	21.21	0.54	0.632	45	0.0075	0.0072	21.07	0.58	0.946
0.0120	0.0092	20.65	0.65	0.590	44	0.0070	0.0062	20.90	1.30	1.072
0.0080	0.0080	20.50	0.73	0.690	43	0.0040	0.0060	20.49	1.00	1.016
0.0040	0.0060				42	0.0070	0.0047	19.75	1.39	1.125
0.0060	0.0055	19.50	0.84		41	0.0030	0.0047	19.18	0.81	1.093
0.0065	0.0060				40	0.0040	0.0033			
0.0055	0.0058				39	0.0030	0.0033	18.50	1.17	
0.0075	0.0057	18.17	0.96		38	0.0030	0.0027			
0.0040	0.0055				37	0.0020	0.0025	17.50		
0.0050	0.0040	17.20	0.63		36	0.0025	0.0018	17.01	0.69	
0.0030	0.0037				35	0.0010	0.0013			
0.0030	0.0027				34	0.0005	0.0008			
0.0020	0.0028				33	0.0010	0.0007			
0.0035	0.0023				32	0.0005	0.0007			
0.0015	0.0023				31	0.0005	0.0005			
0.0020	0.0015				30	0.0005	0.0005			
0.0010	0.0017				29	0.0005	0.0005			
0.0020	0.0013				28	0.0005	0.0003			
0.0010	0.0010				27	0 0000	0.0003			
0.0000	0.0007				26	0.0005	0.0002			
0.0010	0.0007				25	0.0000	0.0002			
0.0010	0.0007				24					
0.0000	0.0005				23					
0.0005	0.0002				22					
0.0000	0.0003				21					
0.0005	0.0002				20					
0.0000	0.0002				19					
0.0000	0.0000				18					
0.0000	0.0000				17					
0.0000	0.0000				16					
0.0000	0.0002				15					
0.0005	0.0002				14					
0.0000	0.0002				13					

Table A-IV. Fractional yields of the emitted particles calculated by the NEM calculation.

	462 MeV		944 MeV		1844 MeV		
Isotope	a=A/10	a=A/20	a=A/10	a=A/20	a=A/10	a=A/20	a=A/20
n	0.628	0.572	0.568	0.516	0.513	0.475	0.4660
H	0.269	0.230	0.231	0.199	0.211	0.194	0.1915
H-2	0.044	0.083	0.076	0.119	0.098	0.136	0.1275
H-3	0.011	0.023	0.035	0.041	0.054	0.056	0.0484
He-3	0.005	0.011	0.022	0.023	0.044	0.033	0.0295
He-4	0.043	0.081	0.067	0.102	0.080	0.106	0.0971
He-6							0.0072
Li-6							0.0102
Li-6*							0.0023
Be-7							0.0049
Be-7*							0.0014
Li-7							0.0096
Li-7*							0.0043
Li-8							0.0001
Li-8*							0.0000
N-13							0.0001

REFERENCES

1. J. M. Miller and J. Hudis, Ann. Rev. Nucl. Sci. 9,159 (1959).
2. B. G. Harvey, Progress Nucl. Phys. 7, 89 (1959).
3. N. A. Perfilov, O. V. Lozhikin, and V. P. Shamov, Usp. Fiz. Nauk 60, 3 (1960): ibid Soviet Phys. Usp. (Engl. Transl.) 3, 1 (1960).
4. E. K. Hyde, A Review of Nuclear Fission, Part Two - Fission Phenomena at Moderate and High Energy, Lawrence Radiation Laboratory Report UCRL-9065, Feb. 1960 (unpublished).
5. H. Feshback, Ann. Rev. Nucl. Sci. 8, 49 (1958).
6. N. Bohr, Nature 137, 344 (1936).
7. R. Serber, Phys. Rev. 72, 1114 (1947).
8. M. Lax. Rev. Mod. Phys. 23, 287 (1951).
9. G. F. Chew, Phys. Rev. 80, 196 (1950).
10. G. F. Chew and M. L. Goldberger, Phys. Rev. 87, 778 (1952).
11. G. F. Chew and G. C. Wick, Phys. Rev. 85, 636 (1952).
12. J. Ashkin and G. C. Wick, Phys. Rev. 85, 686 (1952).
13. S. Ulam and J. Von Neumann, Bull. Am. Math. Soc. 53, 1120 (1947).
14. M. L. Goldgerber, Phys. Rev. 74 1269 (1948).
15. G. Bernardini, E. T. Booth, and S. J. Lindenbaum, Phys. Rev. 85, 826 (1952).
16. J. Combe, Nuovo Cimento 3, 182 (1956).
17. P. Cuer and J. Combe, Compt. Rend. 238, 1799 (1954).
18. Ibid: 239, 351 (1954).
19. J. W. Meadows, Phys. Rev. 98, 744 (1955).
20. H. McManus, W. T. Sharp, and H. Gellman, Phys. Rev. 93, 924 (1954).
21. G. C. Marrison, H. Muirhead, and W. G. V. Rosser, Phil. Mag. 44, 1326 (1953).
22. H. Muirhead and W. G. V. Rossner Phil. Mag. 46, 652 (1955).
23. G. Rüdstam, Spallation of Medium Weight Elements (Thesis), Uppsala University (Uppsala Sweden) (1956)(unpublished).

24. N. Metropolis, R. Bivens, M. Strom, A. Turkevich, J. M. Miller, and G. Friedlander, Phys. Rev. 110, 185 (1958).
25. Ibid: Phys. Rev. 110, 204 (1958).
26. V. Weisskopf, Phys. Rev. 52, 295 (1937).
27. Blatt and V. Weisskopf, Theoretical Nuclear Physics (John Wiley and Sons, New York, 1952).
28. K. J. Le Couteur, Proc. Phys. Soc.(London) 63A, 259 (1950).
29. Ibid. 65A, 718 (1952).
30. Y. Yamaguchi, Progc.Theoret. Phys. (Kyoto) 5, 142 (1950).
31. Y. Fujimoto and Y. Yamaguchi, Progc. Theoret. Phys. (Kyoto) 4, 468 (1949).
32. Ibid. 5, 76, 787 (1950).
33. I. Dostrovsky, P. Rabinowitz, and R. Bivins, Phys. Rev. 111, 1659 (1958).
34. I. Dostrovsky, Z. Fraenkel, and P. Rabinowitz in Proceeding of the Second United Nations International Conference on the Peaceful Uses of Atomic Energy (United Nations, Geneva, 1958), Vol. 15, p. 301.
35. I. Dostrovsky, Z. Fraenkel, and G. Friedlander, Phys. Rev. 116, 683 (1959).
36. I. Dostrovksy, Z. Fraenkel, and L. Winsberg, Phys. Rev. 118, 781 (1960).
37. I. Dostrovsky, Z. Fraenkel, and R. Rabinowitz, Phys. Rev. 118, 791 (1960).
38. I. Dostrovksy, Z. Fraenkel, and J. Hudis, Phys. Rev. 123, 1452 (1961).
39. H. Hirwitz Jr. and H. Bethe, Phys. Rev. 81, 898 (1951).
40. B. D. Pate and A. M. Poskanzer, Phys. Rev. 123, 647 (1961).
41. D. W. Barr, Nuclear Reactions of Copper Induced by 5.7 BeV Protons (Thesis), University of California Radiation Laboratory Report UCRL-3793 May 1957 (unpublished).
42. A. A. Caretto and G. Friedlander, Phys. Rev. 110, 1169 (1958).
43. S. S. Markowitz, F. S. Rowland, and G. Friedlander, Phys. Rev. 112, 1295 (1958).

44. N. T. Porile, Phys. Rev. 125, 1379 (1962).

45. V. P. Crespo, Ejection of Large Fragments in High-Energy Nuclear Reactions (Thesis), Lawrence Radiation Laboratory Report UCRL-9683, September, 1961 (unpublished).

46. A. A. Caretto, J. Hudis, and G. Friedlander, Phys. Rev 110, 1130 (1958).

47. R. Wolfgang, E. W. Baker, A. A. Caretto, J. B. Cumming, G. Friedlander and J. Hudis, Phys. Rev. 103, 394 (1956).

48. F. S. Rowland, and R. L. Wolfgang, Phys. Rev. 110, 175 (1958).

49. E. Baker, G. Friedlander, and J. Hudis, Phys. Rev. 112, 1319 (1958).

50. A. K. Lavrukhina, L. P. Moskuleva, L. D. Krasavina, and I. M. Grechishcheva At. Energ. (U.S.S.R.) 3, 285 (1957): translation Soviet J. At. Energy (Engl. Transl.) Energy 3, 1087 (1957).

51. A. E. Glassgold, W. Heckrotte, and K. M. Watson, Ann. Phys. (N.Y.) 6, 1 (1959).

52. H. Faissner and H. Schneider, Nucl. Phys. 19, 346 (1961).

53. D. I. Blokhintsev, J. Exptl. Theoret. Phys. (U.S.S.R.) 33, 1295 (1957); Soviet Phys. JETP (Engl. Transl.) 6, 995 (1958).

54. D. H. Perkins, Proc. Roy. Soc. (London) 203, 399 (1950).

55. S. O. C. Sörensen, Phil. Mag. 42, 188 (1951).

56. B. H. Smith, K. R. MacKenzie, J. Reidel, Q. Kerns, W. R. Baker, C. W. Park, and R. L. Thorton, The Electrical Aspects of the UCRL 740-MeV Synchrocyclotron, University of California Radiation Laboratory Report UCRL-3779 Rev., October 1957.

57. J. T. Vale, (Lawrence Radiation Laboratory, Berkeley) private communication.

58. G. Igo, (Lawrence Radiation Laboratory, Berkeley) private communication.

59. M. Lindner and R. N. Osborne, Phys. Rev. 91, 342 (1953).

60. W. E. Crandall, G. P. Millburn, R. V. Pyle, and W. Birnbaum, Phys. Rev. 101, 329 (1956).

61. Collected Radiochemical Procedures, Los Alamos Scientific Laboratory Report LA-1721, Los Alamos, New Mexico, December 1954.

62. W. W. Meinke, Chemical Procedures used in Bombardment Work at Berkeley, University of California Radiation Laboratory Report UCRL-432, August 1949 (unpublished).

63. H. Marshall Blann, Fission of Gold with 112-MeV Carbon-12 Ions: A Yield-Mass and Charge-Distribution Study, (Thesis), University of California Radiation Laboratory Report UCRL-9190, May 1960 (unpublished).

64. B. P. Bayhurst and R. J. Prestwood, Nucleonics 17, 82 (1959).

65. R. L. Heath, Scintillation Spectrometry Gamma Ray Spectrum Catalogue, AEC Research and Development Report IDO-16408, 1957.

66. G. R. Keepin, T. F. Wimlet, and R. K. Ziegler, J. Nucl. Energy 6, 1 (1957).

67. W. F. Biller, Characteristics of Bismuth Fission Induced by 340 MeV Protons (Thesis), University of California Radiation Laboratory Report UCRL-2067, December, 1952 (unpublished).

68. Nuclear Data Sheets, National Academy of Sciences, National Research Council (U.S. Government Printing Office, Washington 25, D. C., 1960).

69. D. Strominger, J. M. Hollander, and G. T. Seaborg, Rev. Mod. Phys. 30, 585 (1958).

70. R. D. Evans, The Atomic Nucleus, (McGraw-Hill Book Co., Inc., New York, 1955) p. 762.

71 R. M. Diamond, Phys. Rev. 95, 410 (1954).

72. H. B. Mathur, E. K. Hyde, C. A. Levine, and P. K. Kofstad, Phys. Rev. 97 117 (1955).

73. J. M. Alexander, L. Altman, and S. Howry, Lawrence Radiation Laboratory, Berkeley (unpublished).

74. A. G. W. Cameron, At. Energy Can. Ltd. Report CRP-690, 1957.

75. J. M. C. Scott, Phil. Mag. 45, 441 (1954).

76. J. A. Evans, Proc. Phys. Soc. (London) 73, 33 (1959).

77. B. D. Wilkins, (Lawrence Radiation Laboratory, Berkeley) private communication.

78. L. L. Altman, (Lawrence Radiation Laboratory, Berkeley) private communication.

79. G. Igo and H. Wegner, Phys. Rev. 81, 898 (1951).

80. R. D. Evans, The Atomic Nucleus, (McGraw-Hill Book Co., New York, 1955) p. 749.

81. L. Winsberg, and J. M. Alexander, Phys. Rev. 121, 518 (1961).

82. S. Kaufman, Phys. Rev. 126, 1189 (1962).

83. T. J. Gooding, Nucl. Phys. 12, 241 (1959) .

84. I. M. Ladenbauer and L. Winsberg, Phys. Rev. 119, 1368 (1960).

85. H. A. Bethe and F. de Hoffmann, Mesons and Fields: Volume II, Mesons (Row, Peterson and Co., Evanston, Ill.) p. 321.

86. E. Gardner and C. M. G. Lattes, Science 107, 270 (1948).